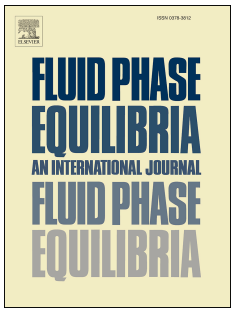

Estimation of the virial coefficients by means of chaotic oscillations of pressure and density: Application to quantum gases with cubic equations of state

Manuel F. Pérez-Polo, Manuel Pérez-Molina, Elena Fernández Varó, Javier Gil Chica

PII: S0378-3812(18)30251-6

DOI: 10.1016/j.fluid.2018.06.015

Reference: FLUID 11870

To appear in: *Fluid Phase Equilibria*

Received Date: 25 March 2018

Revised Date: 17 June 2018

Accepted Date: 25 June 2018

Please cite this article as: M.F. Pérez-Polo, M. Pérez-Molina, Elena.Ferná. Varó, J.G. Chica, Estimation of the virial coefficients by means of chaotic oscillations of pressure and density: Application to quantum gases with cubic equations of state, *Fluid Phase Equilibria* (2018), doi: 10.1016/j.fluid.2018.06.015.

Estimation of the virial coefficients by means of chaotic oscillations of pressure and density: Application to quantum gases with cubic equations of state

Manuel F. Pérez-Polo[a*] Manuel Pérez-Molina[b]; Elena Fernández Varó[c], Javier Gil Chica[d],

[a b d e]Departamento de Física, Ingeniería de Sistemas y Teoría de la Señal, Escuela Politécnica Superior, Universidad de Alicante. [c]Departamento de Óptica, Campus de San Vicente, Alicante, Spain. Fax 965903682. [a]E-mail: manolo@dfists.ua.es [b]E-mail: ma_perez_m@hotmail.com. [c]E-mail: elena.fernandez@ua.es. Phone: +34 965909673, E-mail: gil@dfists.ua.es.

Abstract

This paper analyzes how to determine the virial coefficients B and C of real gases by using a theoretical device whose pressures and densities oscillate in chaotic regime. The device is formed by a valve, a pressure controller, a pressure probe and a gas accumulator, for which the thermodynamic model has been derived from the force-mass-energy balances. This model allows keeping the gas temperature almost constant with chaotic oscillations in the inlet to the accumulator. The chaotic data are used to obtain variability in the pressures and densities, so that they can be used as experimental values from which the virial coefficients are estimated. For this purpose, several cubic and high precision equations of state for polar and non-polar gases and mixtures are used. In particular, the virial coefficient B for dry air is estimated by using high precision state equations, whereas, the virial coefficients B and C are also estimated for quantum gases (He4, He3 H_2, D_2, Ne) by using several modified cubic equations of state at moderate and high pressures. Furthermore, the values for the virial coefficient B obtained from numerical simulations are used to estimate the intermolecular potential and the radial distribution function. The results are in good agreement with the currently known experimental data for virial coefficients published in the literature.

Keywords: Pressure control, virial coefficients, chaotic oscillations, equations of state, quantum gases.

a* Author whose correspondence should be addressed

1 Introduction

In industrial applications, the design of control valves for gases is a well known topic that has been addressed in technical catalogues and books [1-3]. However, despite the great amount of information and expertise available in the field, this knowledge has been little used in the study of the thermodynamics properties of real gases at moderate and high pressures. In addition, the application of chaotic behavior to study the thermodynamic properties of real gases by using devices with control valves is an in interesting field of research which, however, has not been fully explored. In this context, the aim of the present work relies on using a theoretical device for pressure control oscillating in chaotic regime to estimate the virial coefficients and the radial distribution function of several real gases both at moderate and high pressures.

The theoretical device addressed in this paper is formed by a PI controller, a control valve, a pressure probe, connection pipes and an accumulation vessel, and it aims to obtain chaotic oscillations in the pressure and density while maintaining an almost constant temperature at the inlet to the vessel. The model of the device is obtained from the balance equations of forces (control valve) and mass-energy (vessel and connection pipes) in a similar way as that considered in Ref [4], whereas the pressure probe is modeled assuming a nonlinear first-order system. The values of the system parameters have been chosen taking into account those of real devices, whereas the ranges for the proportional constant and the reset time of the PI controller have been chosen from the technical sheets of Design Instrument Series [5].

In the control valve, the inlet gas flow rate is assumed to be isentropic and it is calculated from cubic and high precision state equations [6-9]. Moreover, the device has been designed so that the control valve affects to the thermal subsystem (formed by the vessel accumulator and pipes) but the thermal subsystem has no influence on the control valve. The purpose of this layout is to obtain an adequate volume of the accumulation vessel so that the temperature of the gas contained within it is almost constant and equal to the temperature of the gas at the vessel inlet. This leads to a device which operates at an almost constant temperature but with the possibility of varying chaotically the pressure and density of the gas at the inlet of the vessel due to the plug movement of the nonlinear control valve. The main advantage of this device is that it does not require an

additional system to maintain the gas temperature constant, thus providing a procedure to study the virial coefficients which is simpler than others previously published in the literature [10-11].

On the other hand, it is well known that a possible route to obtain chaotic oscillations may be to obtain a self-oscillating behavior superposed to another oscillating one associated to the harmonic variation of a system parameter [12-13]. In this sense, the self-oscillating behavior in our model has been determined by imposing that the characteristic polynomial corresponding to the linear part of the mechanical subsystem has two purely imaginary roots [14] and varying harmonically the pressure probe time constant.

The proposed device is applied to estimate theoretically the second and third virial coefficients (B and C) for the methane using generalized cubic state equations [15] as well as the second virial coefficient for dry air considering it as a mixture of nitrogen (78.1 %), oxygen (20.95 %), argon (0.92 %) and carbon dioxide (0.03 %). For this purpose, the intermolecular Lennard–Jones potential and a high precision state equation for non-polar (nitrogen, oxygen, argon, carbon dioxide) and polar (ammonia) gases is incorporated to the model by considering variable specific heats with the pressure and temperature. The model can be used for temperatures and pressures above the critical point as well as for temperatures below the critical temperature. For the latter, the pressure oscillations must be smaller than the corresponding saturation pressure at the considered temperature.

Our model is also applied to quantum gases (He4, He3, H_2, D_2, Ne) substituting the critical temperature and pressure by the corresponding effective critical values [16] in the cubic equations of state of Peng-Robinson PR [17-18] and Soave-Rechling-Kwong SRK [18], [19]. This allows to verify that it is possible to reproduce very accurately the experimental values of the second virial coefficient and also the third virial coefficient in certain temperature ranges, both at moderate and high pressures. Other cubic equations such as the ones of Soave S [20-22], Peng-Robinson with translated volume PRT and Van-der-wals with translated volume VDWT [6] are also considered, verifying that in these cases the approximation of the virial coefficients is less accurate at low temperatures. Finally, the radial distribution function in the first-

order approximation is estimated by using an intermolecular potential of Mie type [16] together with the data for the pressures, volumes and temperatures (P,V,T) obtained from the chaotic simulations.

2 Thermodynamic model of the device

Figure 1 shows the layout of the considered device, in which the accumulation vessel has a sufficiently large volume so that the amount of gas in the pipes can be neglected and the pressures are assumed to range from 2 bars up to 100 bars.

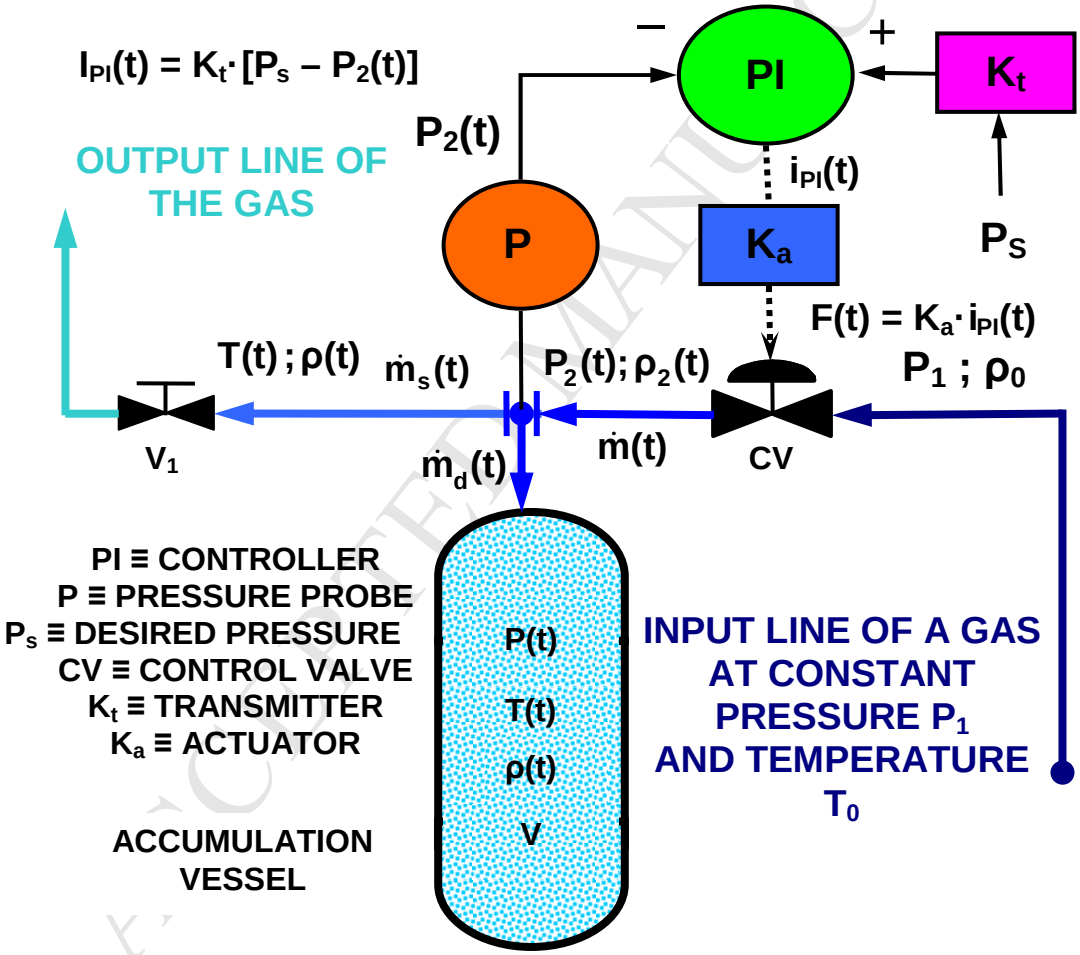

Fig. 1 Schematic layout of the theoretical device, which includes a PI controller, connection pipes, the gas accumulation vessel, the input and output lines and the used nomenclature for the dynamical variables.

A probe which provides the output pressure of the control valve and expels gas out of the device towards the vessel is connected to the latter through a T-shaped connection. It should be pointed out that this device constitutes a simplification of a real

device used for air pressure control built at the University of Alicante. Next, the equations of the mathematical model including both the mechanical and thermal subsystems shall be defined.

i) Model of the control valve plus the control system

The equations of the mechanical subsystem including the control valve and the PI controller are given by [1-5], [10-11]:

$$\frac{dx_1(t)}{dt} = x_2(t) \;\; ; \;\; \frac{dx_2(t)}{dt} = x_3(t)$$
$$\frac{dx_3(t)}{dt} = -\omega_n^2 x_2(t) - 2\delta\omega_n x_3(t) + K_t\left[P_s - P_2(t)\right] - \frac{K_{NL}}{\tau_i} x_1^2(t)\, x_2(t) \qquad (1)$$
$$x(t) = b_0 x_1(t) + b_1 x_2(t)$$

where δ is a damping coefficient (0 < δ < 1), ω_n is the undamped frequency (rad/s) and $x_1(t), x_2(t)$ and $x_3(t)$ are intermediate variables related to the dimensionless displacement of the valve *x(t)* (ranging between 0 for a completely closed valve and 1 for a completely open valve), whose units are indicated in table 1. Furthermore, the term $K_t\left[P_s - P_2(t)\right]$ takes into account the pressure probe, being P_s the desired pressure and $P_2(t)$ the measured pressure (see Fig 1). On the other hand, the nonlinear term $x_1^2(t)\, x_2(t)$ takes into account nonlinearities associated to the measurement process, K_{NL} (see table 1) is a constant that will be of great importance in the analysis of the self-oscillating behavior and τ_i is the reset time (integral action of the PI controller). Finally, the parameters b_0 and b_1 depend on the proportional and the integral constant of the PI controller. The key aspect of this model is that by knowing $P_2(t)$ and the initial conditions for $x_1(t), x_2(t)$ and $x_3(t)$ it is possible to calculate the dimensionless valve position *x(t)* by solving Eqs (1), as it shall be discussed next.

ii) Flow rate in the control valve

The model for the flow rate relies on the assumption of isentropic flow for an ideal gas [4]. The flow rate $Q_2(t)$ (m^3/s) is defined as:

$$Q_2(t)=\frac{G_2(t)}{\rho_2(t)}=\begin{cases}\sqrt{\dfrac{2}{R}}\dfrac{C_f A_0 f\left[x(t)\right]}{\rho_2(t)}\dfrac{\varepsilon}{\sqrt{T_0}}\sqrt{P_2(t)\left[P_1-P_2(t)\right]} \\ \varepsilon=\sqrt{\dfrac{k}{k-1}\dfrac{P_1^2}{P_2^2(t)-P_1^2}\left[\left(\dfrac{P_2(t)}{P_1}\right)^{2/k}-\left(\dfrac{P_2(t)}{P_1}\right)^{k+1/k}\right]}\ ;\ \text{for}\ \dfrac{P_{ch}}{P_1}>\left(\dfrac{2}{k+1}\right)^{k/k-1} \\ \dfrac{C_f A_0 f\left[x(t)\right]}{\rho_2(t)}\dfrac{P_1}{\sqrt{RT_0}}\cdot\sqrt{k\left(\dfrac{2}{k+1}\right)^{k+1/k-1}}\ ;\ \text{for}\ \dfrac{P_{ch}}{P_1}\le\left(\dfrac{2}{k+1}\right)^{k/k-1}\end{cases} \tag{2}$$

where ε is the so called expansion coefficient, C_f is the valve discharge coefficient ranging between 0.68 and 0.9, A_0 is a characteristic area of the valve (in m^2) and T_0 is the inlet gas temperature in K. Besides, $k = c_p(T)/c_v(T)$ being $c_p(T)$ and $c_v(T)$ the specific heats at constant pressure and volume respectively (which depend on the temperature), R is the specific constant of a given gas, P_1 and $P_2(t)$ are the input and output pressures respectively and P_{ch} is the pressure from which when $P_2(t) \equiv P_{ch}$ the flow is choked, i.e. the gas mass flow $G_2(t) = Q_2(t).\rho_2(t)$ (kg/s) remains constant for $P_{ch} \le r_p^* P_1 \Rightarrow P_{ch} \le (2/k+1)^{k/k-1} P_1$. For example, for air at low pressure whose behavior can be regarded as ideal, it is verified that $k = 1.4$ and $P_{ch} \le 0.528 P_1$. This means that if the downstream pressure is below $0.528 \cdot P_1$ then the gas velocity is sonic and the pressure $P_2(t)$ has no influence on the mass flow of the gas. Furthermore, it is assumed that the values of the plug position $x(t)$ and $f[x(t)]$ are given by:

$$f\left[x(t)\right]=x(t)=b_0 x_1(t)+b_1 x_2(t) \tag{3}$$

For non-ideal gases, the corresponding state equation (cubic or high precision state equations) must be considered in Eq (2).

iii) Model of the pressure probe

The output pressure $P_2(t)$ of the control valve is assumed to fulfill the nonlinear differential equation given by:

$$T_m \frac{dP_2(t)}{dt} + P_2(t) = K_m Q_2(t) \tag{4}$$

where T_m is a time constant and K_m *(N/m^2)/(m^3/s)* is a parameter which will be regarded either as constant or time-dependent, as it shall be discussed later. It should be remarked that Eqs (1)-(4) provide the mathematical model of the control valve together with the PI controller taking into account the gas flow rate in the control valve given in Eq (2).

iv) Model of the thermal subsystem

Taking into account the scheme of Fig 1 and assuming that the gas density in the output pipe is equal to the gas density within the vessel, the following mass balance equation can be written:

$$V \frac{d\rho(t)}{dt} = \dot{m}(t) - \dot{m}_s(t) \; ; \; \begin{cases} \dot{m}(t) = Q_2(t)\rho_2(t) \\ \dot{m}_s(t) = Q_s(t)\rho(t) \end{cases} \tag{5}$$

where V is the vessel volume, $\rho(t)$ is the gas density (kg/m^3) within the vessel and $\dot{m}(t)$ and $\dot{m}_s(t)$ (kg/s) are the mass flow rates in the input and output pipes respectively. On the other hand, assuming that the heat losses in the vessel and the heat stored in the vessel walls are both negligible, the energy balance equation for the vessel gas can be written as:

$$Vc_v \frac{d\left[\rho(t)T(t)\right]}{dt} = \dot{m}(t)c_p T_0 - \dot{m}_s(t)c_p T(t) \tag{6}$$

where c_v and c_p (J/kg·K) are the gas specific heats at constant volume and pressure respectively. By expanding the derivative of Eq (6) and substituting Eq (5) into Eq (6) it is deduced that:

$$\frac{dT(t)}{dt} = \frac{\rho_2(t)Q_2(t)}{Vc_v\rho(t)}\left[c_p T_0 - c_v T(t)\right] - \frac{\rho(t)Q_s(t)T(t)}{Vc_v\rho(t)}\left(c_p - c_v\right) \tag{7}$$

Besides Eqs (5) and (7), it is necessary to take into account the following mass balance (see Fig 1):

$$\dot{m}(t) = \dot{m}_d(t) + \dot{m}_s(t) \Rightarrow \rho_2(t) Q_2(t) = \rho_2(t) Q_d(t) + \rho(t) Q_s(t) \tag{8}$$

where the densities $\rho_2(t)$ and $\rho(t)$ are calculated from the state equation of the gas and $Q_d(t)$ is the gas flow rate of the vessel, which is regarded as positive when the gas enters the vessel (see Fig 1) and negative when the gas leaves the vessel. Such gas flow rate is modeled as:

$$Q_d(t) = \begin{cases} K_d \sqrt{P_2(t) - P(t)} & \text{if } P_2(t) > P(t) \\ K_d \sqrt{P(t) - P_2(t)} & \text{if } P(t) > P_2(t) \end{cases} \tag{9}$$

where K_d represents a discharge coefficient. Eqs (5)-(9) constitute the thermal subsystem equations [4], for which the parameter values and units are indicated in table 1.

3 Self-oscillating and chaotic behavior to obtain the virial coefficients

In this section we shall study how to obtain the self-oscillating behavior and how can it be transformed into a chaotic dynamic by varying harmonically the time constant T_m of the pressure probe (see Eq (4)). Once the chaotic behavior has been obtained, it will be analyzed how to determine the second and third virial coefficients by using cubic equations of state (see the Appendix). For this purpose, the system equations are first rewritten by introducing the following new variables:

$$\begin{gathered} x_1'(t) = x_1(t) - x_{1e} \;;\; x_2'(t) = x_2(t) - x_{2e} = x_2(t) \;\;;\;\; x_3'(t) = x_3(t) - x_{3e} = x_3(t) \\ P_2'(t) = P_2(t) - P_s \;\;;\;\; x'(t) = x(t) - x_e = b_0 x_1'(t) + b_1 x_2'(t) \;\;;\;\; x_e = b_0 x_{1e} \end{gathered} \tag{10}$$

where x_{1e}, x_{2e}, x_{3e} and x_e denote the equilibrium point of the system, which is obtained by equating the derivatives of Eq (1) and (5) to zero. The system equations can be expressed in terms of the variables defined in Eqs (10) as:

$$
\left.
\begin{aligned}
\dot{x}_1(t) &= x_2'(t) \quad ; \quad \dot{x}_2(t) = x_3'(t) \\
\dot{x}_3(t) &= -\omega_n^2 x_2'(t) - 2\delta\omega_n x_3'(t) - \left(K_{NL}/\tau_I\right)\left[x_1'(t) + x_{1e}\right]^2 x_2'(t) - K_t P_2'(t) \\
\dot{P}_2(t) &= -\left(1/T_m\right) P_2'(t) + \left(K_m/T_m\right) Q_2(t) \;\; ; \;\; \rho_2(t) = f_2\left[P_2(t), T_0\right] \\
x'(t) &= b_0 x_1'(t) + b_1 x_2'(t) \;\; ; \;\; \rho_2(t) Q_2(t) = \rho_2(t) Q_d(t) + \rho(t) Q_s(t) \\
Q_d(t) &= K_d \sqrt{P_2(t) - P(t)} \quad \text{for} \quad P_2(t) > P(t) \\
Q_d(t) &= K_d \sqrt{P(t) - P_2(t)} \quad \text{for} \quad P(t) > P_2(t) \\
\dot{\rho}(t) &= \left(1/V\right)\left[\rho_2(t) Q_2(t) - \rho(t) Q_s(t)\right] \;\; ; \;\; P(t) = f\left[\rho(t), T(t)\right] \\
\dot{T}(t) &= \frac{\rho_2(t) Q_2(t)}{V c_v \rho(t)}\left[c_p T_0 - c_v T(t)\right] - \frac{\rho(t) Q_s(t) T(t)}{V c_v \rho(t)}\left(c_p - c_v\right)
\end{aligned}
\right\} \qquad (11)
$$

where $Q_2(t)$ is defined by Eqs (2) whereas f_2 and f are the nonlinear functions which respectively relate the density and the pressure with the other state variables according to the equation of state.

Eqs (11) describe the dynamic behavior of the system formed by the control valve (the first four equations) and the accumulation vessel (the last two equations). From a conceptual point of view, the device works in the following way: From the first four equations it determines the pressure $P_2(t)$ at the output of the control valve by setting a temperature T_0, a pressure P_1 at the input of the device and a set pressure P_s. Then with the values of $P_2(t)$, T_0 and the equation of state, the density $\rho_2(t)$ at the output of the control valve is determined.

The density and temperature in the vessel are calculated with the last two Eqs of (11), and the pressure is calculated through the equation of state. Since we want to determine the virial coefficients B and C at the temperature T_0, the temperature of the gas in the vessel must be kept close to T_0. This is achieved by increasing the vessel volume, which leads to approximately constant values for $\rho(t)$ and $T(t)$ since both $d\rho(t)/dt$ and $dT(t)/dt$ are approximately zero in accordance with Eqs (11).

TABLE 1 DEFINITION OF VARIABLES AND PARAMETER VALUES

Variable	Description	Value
P_1	Input pressure (N/m^2)	$2\cdot10^5$ to $8\cdot10^6$
P_s	Pressure set point (N/m^2)	$< P_1$
$P_2(t)$	Pressure in the control valve (N/m^2)	$1\cdot10^5$ to $10\cdot10^6$
$\rho_2(t)$	Density in the control valve (kg/m^3)	1 to 15
T_0	Inlet gas temperature (K)	2.6-900
T(t)	Gas temperature in the vessel (K)	2.6-900
$\rho(t)$	Gas density in the vessel (kg/m^3)	0.9 to 14
P(t)	Pressure in the vessel (N/m^2)	$\leq P_2(t)$
τ_I	Integral time of the PI controller (min)	0-900
K_{NL}	Constant of nonlinear term ($1/mA^2\cdot s^6$)	$8\cdot10^{-4}$ to 8
K_t	Transmitter constant ($mA/N/m^2$)	$3\cdot10^{-5}$ to $3.2\cdot10^{-6}$
V	Vessel volume (m^3)	0.001-1
ω_n	Natural frequency of the control valve (rad/s)	0.69
δ	Damping coefficient of the control valve	$0 < \delta < 1$ (0.26)
K_a	Force constant ($F(t) = K_a\cdot i_{PI}(t)$) (N/mA)	0.3125
b_0	Parameter of the valve plug position ($1/mA\cdot s^3$)	0.01 to 10
b_1	Parameter of the valve plug velocity ($1/mA\cdot s^2$)	$\leq b_0/10$
T_m	Time constant of the pressure probe (s)	5-10
T_{mv}	Fixed value of the time constant (s)	
A_{Tm}	Amplitude of the harmonic disturbance (s)	$< T_{mv}$
ω_{Tm}	Frequency of the harmonic disturbance (rad/s)	0.8-1.2
K_m	Constant of the pressure probe $(N/m^2)/(m^3/s)$	$2\cdot10^{-11}$ to $4\cdot10^{-10}$
C_f	Coefficient of the control valve	0.75
A_0	Control valve area (m^2)	$4\cdot10^{-6}$
ε	Control valve expansion factor	≈ 0.98
x(t)	Dimensionless control valve displacement	$0 \leq x(t) \leq 1$
$Q_2(t)$	Inlet gas flow rate (m^3/s)	$5\cdot10^{-5}$ to $2.5\cdot10^{-4}$
$Q_d(t)$	Gas flow rate to the vessel (m^3/s)	$< Q_2(t)$
$Q_s(t)$	Outlet gas flow rate to the atmosphere (m^3/s)	
K_d	Constant of the flow rate $Q_d(t)$ $(m^3/s)/(N/m^2)^{0.5}$	$5\cdot10^{-9}$ to $1\cdot10^{-7}$
$x_1(t)$	State variable ($mA\cdot s^3$)	
x_{1e}	Equilibrium point of the state variable $x_1(t)$	
$x_2(t)$	State variable ($mA\cdot s^2$)	
$x_3(t)$	State variable ($mA\cdot s$)	
c_p	Specific heat at constant pressure (J/mol)	
c_v	Specific heat at constant volume (J/mol)	
$k = c_p/c_v$	Polytropic coefficient	

3.1 Analysis of self-oscillating behavior

From Eqs (16) it is clear that the equations of the valve, controller and pressure probe defined by the variables $x_1'(t), x_2'(t), x_3'(t)$ and $P_2'(t)$ influence on $\rho(t)$ and $T(t)$, but the dynamics of the mechanical subsystem is independent from the thermal subsystem. Therefore, the linear part of the mechanical subsystem can be obtained by taking the linear terms of the Taylor series around the equilibrium point, which can be written as:

$$\begin{bmatrix} \dot{x}_1'(t) \\ \dot{x}_2'(t) \\ \dot{x}_3'(t) \\ \dot{P}_2'(t) \end{bmatrix} = \begin{bmatrix} 0 & 1 & 0 & 0 \\ 0 & 0 & 1 & 0 \\ 0 & -a_{32} & -2\delta\omega_n & -K_t \\ b_0 A_i & b_1 A_i & 0 & B_i \end{bmatrix} \begin{bmatrix} x_1'(t) \\ x_2'(t) \\ x_3'(t) \\ P_2'(t) \end{bmatrix} \quad ; \quad a_{32} = \omega_n^2 + \frac{K_{NL}}{\tau_i} x_{1e}^2 \tag{12}$$

where the coefficients A_i and B_i are defined as follows:

$$F\left[x_1'(t), x_2'(t), P_2'(t)\right] = -\frac{\left[P_2'(t) + SP\right]}{T_m} + \frac{K_m}{T_m} Q_2'(t)$$

$$A_i b_0 = \left(\frac{\partial F}{\partial x_1'}\right)_e \quad ; \quad B_i b_1 = \left(\frac{\partial F}{\partial P_2'}\right)_e \tag{13}$$

The characteristic polynomial of Eq (12) is given by:

$$P(s) = |sI - A| = s^4 + a_3 s^3 + a_2 s^2 + a_1 s + a_0$$

$$a_3 = 2\delta\omega_n - B \; ; \; a_2 = \omega_n^2 + \frac{K_{NL}}{\tau_i} x_{1e}^2 - 2\delta\omega_n B \; ; \; a_1 = b_1 A K_t - \left(\omega_n^2 + \frac{K_{NL}}{\tau_i} x_{1e}^2\right) B \; ; \; a_0 = b_0 A K_t \tag{14}$$

On the other hand, assuming that the coefficients of the characteristic polynomial given by Eqs (14) are positive -i.e. $a_i > 0$ *(i=0,1,2,3)*-, a necessary condition for self-oscillation is [14]:

$$\left(\frac{a_2 a_3 - a_1}{a_3}\right) a_1 = a_0 a_3 \tag{15}$$

Under the self-oscillation condition of Eq (15), the characteristic polynomial of Eq (12) can be rewritten as:

$$P(s)=\left(s^2+\frac{a_1}{a_3}\right)\left[s^2+a_3 s+\left(a_2-\frac{a_1}{a_3}\right)\right]\Rightarrow\begin{cases}s_{1,2}=\pm j\sqrt{\dfrac{a_1}{a_3}}\\ s_{3,4}=\dfrac{-a_3\pm\sqrt{a_3^2-4\left(a_2-\dfrac{a_1}{a_3}\right)}}{2}\end{cases}\tag{16}$$

To ensure that the roots $s_{3,4}$ of Eq (16) are complex conjugate with negative real part, the following additional condition must be fulfilled:

$$a_3^2<4\left(a_2-a_1/a_3\right)\Rightarrow a_3<4a_0/a_1\tag{17}$$

Consequently, as per Eqs (14)-(17) it is possible to choose a value for the parameter K_{NL} to obtain of a pair of purely imaginary roots (roots $s_{1,2}$ in Eq (16)) that lead to self-oscillating behavior, as it will be analyzed later.

Next we are to consider how to estimate the virial coefficients by resolving numerically Eqs (11) with the self-oscillation conditions given by Eqs (15) and (17) assuming a cubic state equation, which in generalized form can be written as [15]:

$$z=\frac{Pv}{RT}=\frac{v}{v-b}-\frac{\left[\Theta(T)/RT\right]v(v-\eta)}{(v-b)\left(v^2+\delta_1 v+\varepsilon\right)}\tag{18}$$

where $\Theta(T)$, η, δ_1 and ε depend on the particular cubic state equation that is considered. A summary of several cubic state equations can be found in Refs [6-7,15]. For example, considering the SRK state equation we have that:

$$P=\frac{RT}{v-b}-\frac{a\alpha(T_r)}{v(v+b)}\ \ ;\ \ \Theta(T)=a\alpha(T_r)\tag{19}$$

where the values of *a*, *b* and $\alpha(T_r)$ are given in the Appendix. It should be recalled that the specific heats at constant volume and pressure (c_v and c_p respectively) in Eqs (11) must be calculated assuming a non-ideal gas behavior, i.e. by using the relations:

$$c_v(t) = R - c_p\left[T(t)\right] \quad ; \quad c_p\left[T(t)\right] = A_1 + A_2T(t) + A_3T^2(t) + A_4T^3(t) + A_5T^4(t) \quad (20)$$

where *T(t)* is the gas temperature in the vessel and the coefficients A_i (i=1,2,3,4,5) can be found in the literature for each gas [24]. As per Eqs (19) and (20) it follows that:

$$c_v = c_p^* - R - T\frac{\partial^2\Theta}{\partial T^2}\int_{\infty}^{v}\frac{dv}{v^2+\delta_1 v+\varepsilon} \quad ; \quad c_p - c_v = \frac{Tv\beta_c^2}{\kappa_c} \quad (21)$$

where c_p^* is the specific heat calculated as if the gas was ideal, whereas $\beta_c = (1/v)(\partial v/\partial T)_P$ and $\kappa_c = -(1/v)(\partial v/\partial P)_T$ are the isobaric expansion coefficient and the isothermal compressibility coefficient respectively, which can be calculated from the cubic equation of state. In contrast with the case of an ideal gas in which the calculation of the specific volume is trivial, in our system the following cubic equation must be solved in each simulation step:

$$v^3 + \left(\delta_1 - b - \frac{RT}{P}\right)v^2 + \left(\varepsilon - b\delta_1 - \frac{\delta_1 RT}{P} + \frac{\Theta(T)}{P}\right)v - \frac{\Theta(T)\eta}{P} - b\varepsilon - \frac{\varepsilon RT}{P} = 0 \quad (22)$$

where the largest positive root must be chosen in Eq (22).

Once the simulation data are obtained, the key point is that the self-oscillating pressures, specific volumes and temperatures can be used as if they were experimental data to obtain the virial coefficients. The virial equation can be written as:

$$v\left(\frac{Pv}{RT} - 1\right) = B(T) + \frac{C(T)}{v} + \frac{D(T)}{v^2} + \frac{E(T)}{v^3} + ... \quad (23)$$

where *B(T), C(T), D(T)* and *E(T)* are the second, third and so on virial coefficients. It is interesting to remark that currently there are not experimental data for the coefficients *D(T)* and *E(T)* and those of higher order, so only the coefficients *B(T)* and *C(T)* have been estimated from the simulated data obtained in self-oscillation for different input temperatures T_0 (see Fig 1).

It should be remarked that the uncertainties of the proposed method to estimate the virial coefficients B(T) and C(T) are associated to the numerical integration method, which has a local error proportional to the simulation step raised to four and thus can be considered as acceptable. In addition, the model is numerically rather stable due to the limitation in the dimensionless valve plug motion (between 0 and 1) and the limitation of the pressures (choked pressures). Consequently, the data obtained from the numerical simulations allow to estimate B(T) and C(T) by least-square polynomial fitting of the equation $y = B(T) + C(T)\,x$, where $y = v\left(Pv/RT - 1\right)$ and $x = 1/v$ as per equation (23).

It is very important to remark that this procedure provides accurate values only if the gas behavior is nearly isotherm. Consequently, several simulations are carried out with different input temperatures T_0, and the virial estimations are calculated with the simulation data obtained at the output of the control valve, i.e. with $P_2(t)$ and $\rho_2(t)$ (see Fig 1). The proposed estimation works properly if the vessel temperatures *T(t)* are almost constant and very close to the value of T_0 in each simulation. For this purpose, the vessel volume must be sufficiently large so that the densities and temperatures of the gas inside the vessel vary slowly with time in accordance with Eqs (5) and (7), as it will be analyzed next.

To estimate the virial coefficients for the methane and the argon [22,23], Eqs (11) are numerically solved by using the Soave-Redlich-Kwong (SRK) cubic state equation [19] and assuming the self-oscillation conditions given by Eqs (15)-(17). To do this aim, the fourth-order Runge-Kutta integration method is used with simulation times between 100 and 500 s and with simulation steps T between 0.01 and 0.001 s. An interesting aspect of the numerical procedure is that the system is rather stable due to the limitation in the dimensionless valve plug excursion (between 0 and 1) and the limitation due to the choked pressures values. In addition, to simplify the calculation of

the equilibrium point, the parameter ε in Eq (9) (which is close to 0.98) is linearized as follows:

$$\begin{gathered}\varepsilon=\varepsilon_e \approx \varepsilon\big]_{r_p^*}+\bar{b}\left[\frac{P_2(t)}{P_i}-r_p^*\right]\ ;\ r_p^*=\frac{P_{ch}}{P_1}=\left(\frac{2}{k+1}\right)^{k/(k-1)}\ ;\ k=\frac{c_p(T)}{c_v(T)}\\ \varepsilon\big]_{r_p^*}=\sqrt{\frac{k}{k-1}\frac{1}{r_p^*-r_p^{*2}}\left[\left(r_p^*\right)^{2/k}-\left(r_p^*\right)^{(k+1)/k}\right]}\ ;\ \bar{b}=\frac{1-\varepsilon\big]_{r_p^*}}{1-r_p^*}\ \text{ for }\ \frac{P_2(t)}{P_i}\geq r_p^*\end{gathered} \tag{24}$$

where P_{ch} is the choked pressure obtained from the values of P_1 and the specific heats of the considered gas (which are calculated from Eqs (20) and (21)).

According to Eqs (1)-(4) and (24), the equilibrium point for the mechanical subsystem is defined as:

$$\begin{gathered}x_{2e}=x_{3e}=0\ ;\ P_{2e}=P_s\ ;\ f[x_e]=b_0x_{1e}\\ Q_{2e}=\sqrt{\frac{2}{R}}\frac{C_fA_0f[x_e]}{\rho_{2e}}\frac{\varepsilon_e}{\sqrt{T_0}}\sqrt{P_s(P_1-P_s)}\ ;\ \text{for } P_1>P_s\ ;\ P_s>P_{ch}\\ -\frac{P_s}{T_m}+\frac{K_m}{T_m}Q_{2e}=0\Rightarrow Q_{2e}=\frac{P_s}{K_m}\end{gathered} \tag{25}$$

On the other hand, the equilibrium point for the thermal subsystem is calculated from Eqs (5)-(7) as follows:

$$\begin{gathered}\rho_{2e}Q_{2e}=\rho_{2e}Q_{de}+\rho_eQ_{se}\ ;\ Q_{de}=0\\ Q_{de}=\begin{cases}K_d\sqrt{P_s-P_e}\ ;\ \text{for}\ P_s>P_e\\ K_d\sqrt{P_e-P_s}\ ;\ \text{for}\ P_s<P_e\end{cases}\\ 0=\frac{\rho_{2e}Q_{2e}}{c_v\rho_e}\left[c_pT_0-c_vT_e\right]-\frac{\rho_eQ_{se}T_e}{c_v\rho_e}\left(c_p-c_v\right)\Rightarrow T_e=T_0\end{gathered} \tag{26}$$

where the gas density in Eqs (25) and (26) is calculated from the state equation of a real gas (see Eq (18)).

The simulation results for the methane and the argon are shown in Figs 2 and 3 by using ten temperatures and their corresponding equilibrium values (which are shown

in table 2 for the methane) and taking values for T_m in Eq (11) between 5 and 10 seconds. The values for K_{NL} have obtained assuming that the self-oscillation conditions given by Eqs (15)-(17) are fulfilled and calculating the values of x_{1e} from Eq (25).

TABLE 2 EQUILIBRIUM POINTS AND SIMULATION VALUES FOR THE METHANE

P_1 = 100 MPa **; P_s** = 60 Mpa **; δ** =0.26 **; ω_n** = 0.69 rad/s **; b_0** = 3 mA·s^{-3}

b_1 = 0.03 mA· s^{-2}**; V** = 10^{-3} m^3 **K_d** = 6.10^{-9} $m^3/s/(N/m^2)^{0.5}$**; K_t** = $6.4.10^{-8}$ $(1/N/m^2)$

K_m = $4.8140.10^{-11}(N/m^2)/(m^3/s)$

T_0 (K)	T_m (s)	x_e	$K_{NL}.10^6$ $1/mA^2 \cdot s^6$	x_{1e} $mA \cdot s^3$	ρ_{2e} (kg/m^3)	n_v mol
200	5	0.1242	1.8672	0.0414	418.3528	20.0770
255.55	5.55	0.1125	2.1599.	0.0375	378.6929	23.6049
311.11	6.11	0.1015	2.5372.	0.0338	341.7617	213031
366.66	6.66	0.0918	2.9917	0.0306	308.0884	19.2600
422.22	7.22	0.0834	3.5127	0.0278	280.7617	17.5006
477.77	7.77	0.0763	4.0892	0.0254	256.7932	16.0056
533.33	8.33	0.0702	4.7123	0.0234	236.4927	14.7412
588.88	8.88	0.0651	5.3752	0.0217	219.2262	13.6649
644.44	9.44	0.0607	6.0736	0.0202	204.4284	12.7425
700	10	0.0569	6.8043	0.0190	191.6331	11.9450

Fig 2 a) shows the self-oscillating pressures $P_2(t)$ measured by the pressure probe shown in Fig 1, where the choked pressures are the approximately straight lines indicated by P_{ch}. On the other hand, Fig 2 b) shows the densities $\rho_2(t)$ which are used in Eq (30) ($P \equiv P_2$; $v = M/\rho_2$; $M \equiv$ molecular mass) to estimate the virial coefficients B and C, whereas Figs 2 c) and 2 d) show the estimated values of the virial coefficients compared to the experimental ones. It should be noted that the virial coefficients estimation cannot be regarded as acceptable for all temperatures due to their self-oscillating behavior. This is due to the fact that the vessel volume is very small (V = 10^{-3} m^3) and therefore the gas temperature in the vessel is not constant, as it can be observed in the three input temperatures T_0 of Fig 3 a) for the argon.

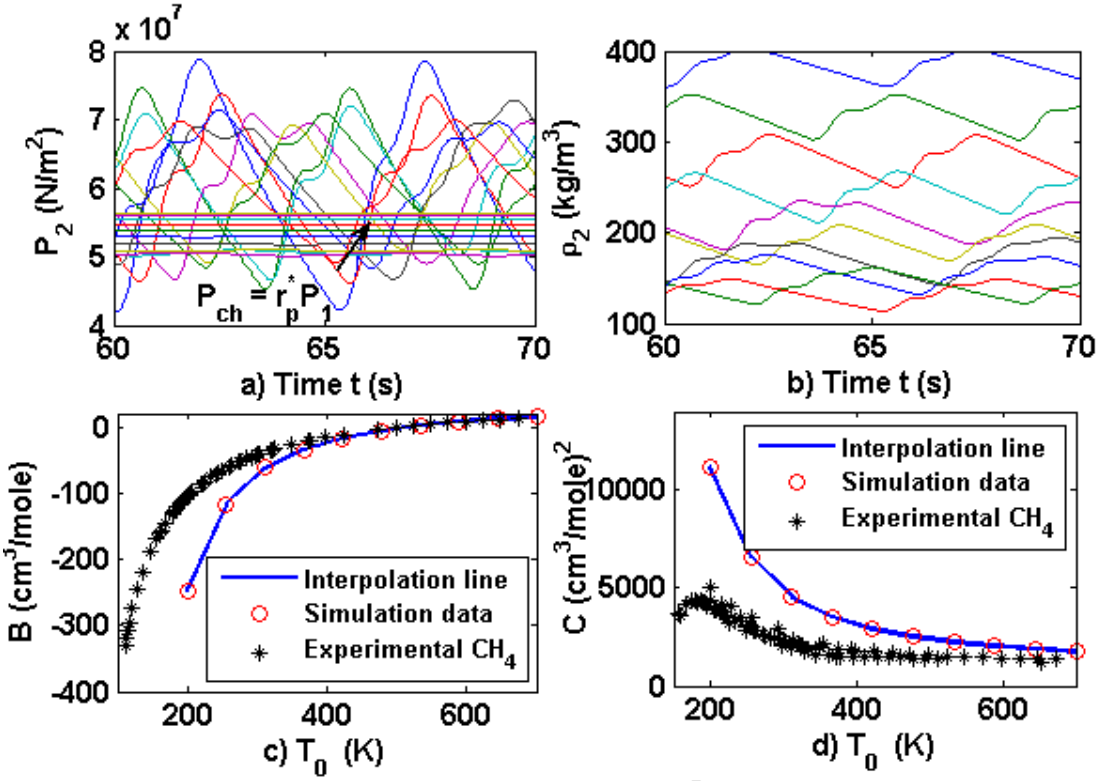

Fig. 2 a) Self-oscillating values of $P_2(t)$ measured by the pressure probe (see Fig 1) for each input temperature T_0, being P_{ch} are the choked pressure for each temperature. b) Self-oscillating densities $\rho_2(t)$ for each pressure $P_2(t)$ and input temperature T_0. c) Estimated values of the virial coefficient B for the methane from the values shown in panels a) and b). d) Estimated values of the virial coefficient C for the methane from the values shown in panels a) and b).

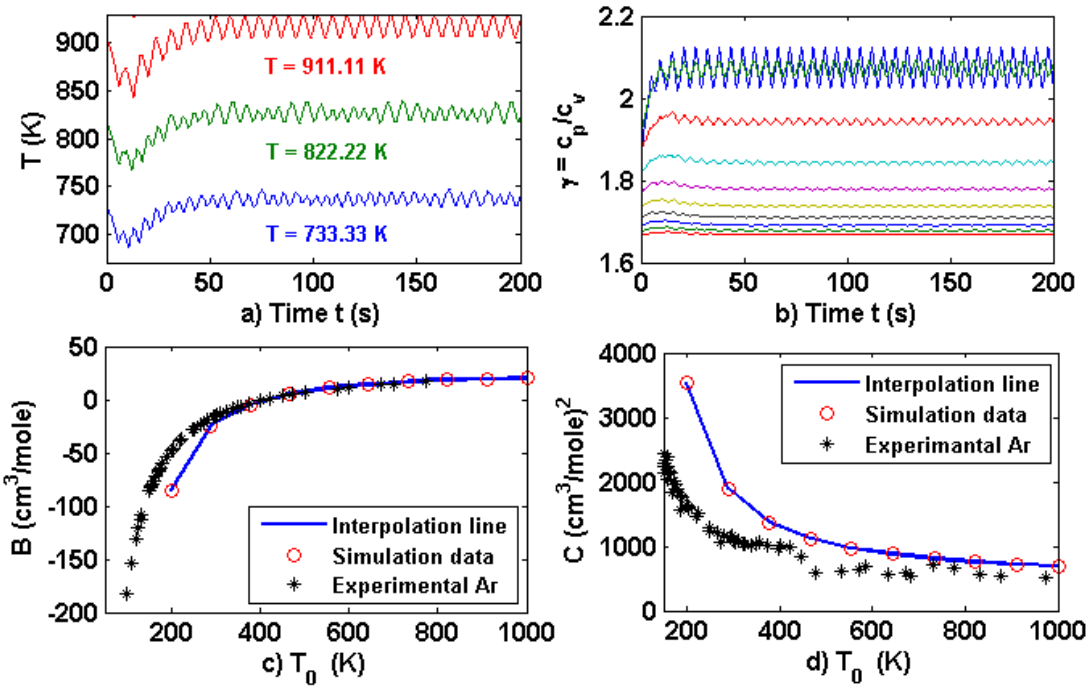

Fig. 3 a) Self-oscillating values of three vessel temperatures Tvi. b) Self-oscillating values of $k = c_p(T)/c_v(T)$ for each input temperature T_0. c) Estimated values of the second virial coefficient B for the argon. d) Estimated values of the third virial coefficient C for the argon.

In Fig 3 b) the exponents $k = c_p(T)/c_v(T)$ obtained from Eqs (2) and (24) are plotted as function of the simulation time, which allows to appreciate clearly the self-oscillating behavior. Furthermore, in Figs 3 c) and d) the virial coefficients are also estimated for the argon, and in this case only the values of the virial coefficient B at high temperatures may be regarded as acceptable.

The previous estimations can be improved by achieving more variability in the simulation data. Taking into account that the model is highly nonlinear, we shall search for chaotic oscillations. The first consideration is that currently there is not a systematic procedure to assure that an oscillating behavior is chaotic. Consequently, we have considered several tests which viewed all together allow us to affirm if a system behavior is chaotic or not with a reasonably high degree of certainty. For this purpose, it has been verified that there appears sensitive dependence, a positive Lyapunov exponent and a power spectral density such that, altogether, are consistent with chaotic behavior.

It is well known that when the matrix of the linearized system at the equilibrium point has two purely imaginary conjugate roots (as it was discussed in the previous section), a harmonic disturbance or the harmonic variation of a system parameter may lead to chaotic dynamics. On the basis of this idea, we assume that the time constant of the pressure probe is harmonically varied in accordance with the following equation:

$$T_m(t) = T_{mv} + A_{Tm}\sin(\omega_{Tm}t) \;\; ; A_{Tm} < T_{mv} \Rightarrow T_m(t) > 0 \tag{27}$$

where A_{Tm} and ω_{Tm} are the amplitude and the angular frequency respectively, and in addition it must be fulfilled that $T_{mv} > A_{Tm}$. Therefore, we aim to verify if the chaotic behavior appears for certain values of AT_m and ω_{Tm} so that the chaotic simulation data can be used to estimate the virial coefficients. It should be remarked that this methodology is aimed to provide an approach whose main motivation is that chaotic dynamics is an inherent property of many dynamical systems like the considered one in our manuscript. Therefore, an advantage of our approach is that it provides a route to estimate the virial coefficients relying only on a set of chaotic measurements.

Fig 4 shows the estimation of virial coefficients B and C for the nitrogen through chaotic behavior by applying a disturbance in the time constant of the pressure probe T_m, as indicated in Eq (27). In this case, ten temperatures T_0 between 200 and 650 K are considered with the parameter values $P_1 = 8{\cdot}10^6$ N/m^2, $P_s = 6{\cdot}10^6$ N/m^2, $V = 1$ m^3, $K_m = 1.9256{\cdot}10^{10}$ (N/m^2)/(m^3/s), $\delta = 0.26$, $\omega_n = 0.69$ rad/s, $K_t = 3.210^{-6}$ (mA/N/m^2), $b_0 = 10$ (1/mA$\cdot$s^3) and $b_1 = 0.1$ (1/mA$\cdot$s^2). In accordance with Eq (34), the disturbance is defined by considering ten values of T_{mv} varying uniformly between 5 and 10, $\omega_{Tm} = 0.8$ rad/s and $A_{Tm} = T_{mv}/fTm$ s, where fTm are other ten values varying uniformly between 1.2 and 1.8. The purpose of this particular choice is to obtain chaotic behavior in all ranges of temperatures T_0.

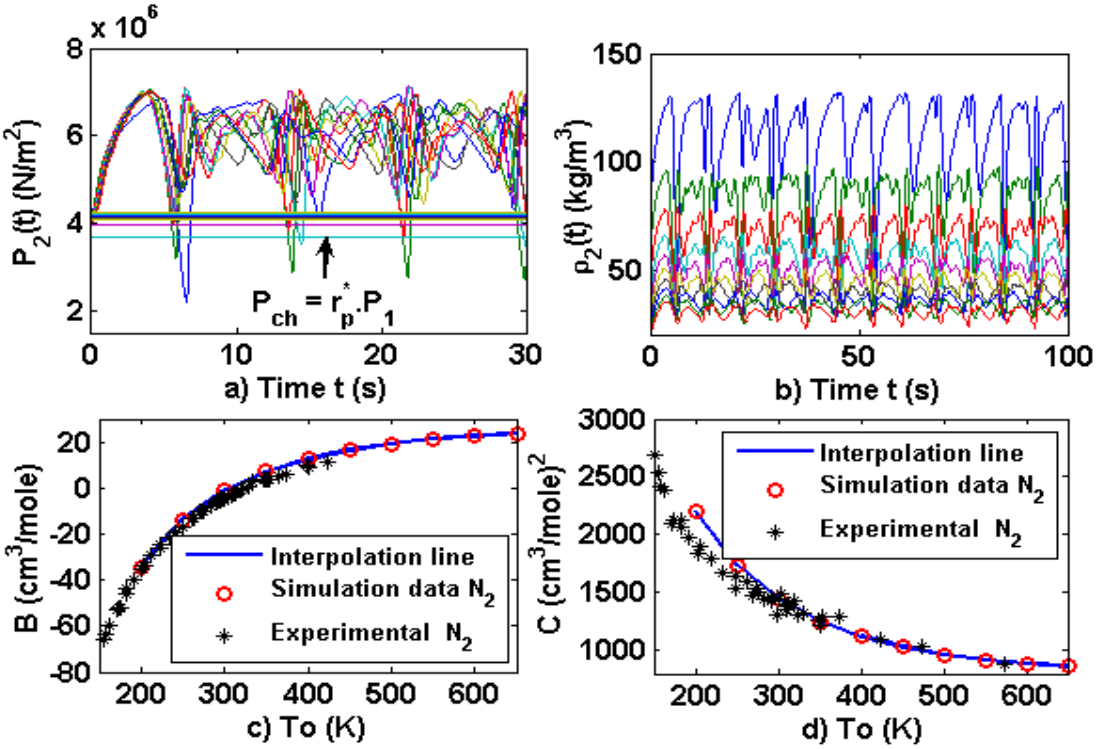

Fig. 4 a) Pressures $P_2(t)$ as a function of time for the nitrogen calculated in self-oscillating regime and at high pressure for ten constant temperatures between *200* and *650* K, being P_{ch} the choked pressures for each temperature. b) Densities $\rho_2(t)$ for the same constant temperatures. c) Simulated chaotic data for the second virial coefficient B of the nitrogen as a function of the temperature. d) Simulated chaotic data for the third virial coefficient C of the nitrogen as a function of the temperature.

The values of K_{NL} have been chosen assuming the conditions of Eqs (15)-(17) (in similar way to the one shown in table 2) so that the self-oscillation appears for each temperature T_0. In Figs 4 a) and b), the pressures $P_2(t)$ and densities $\rho_2(t)$ are plotted showing chaotic oscillations, whereas Figs 4 c) and d) show the estimation of virial coefficients B and C. In this case, it is clear that the estimation of B is similar (with an

error of 5 % around the Boyle temperature when $B = 0$) to the one of Fig 3, while the estimation of C is better at all temperatures T_0.

To corroborate that the gas temperature is approximately constant, we use the simulation data of Fig 4 for the nitrogen and calculate the per cent relative error between T_0 (ranging between 200 and 650 K) and the gas temperature T(t), i.e. $Er = 100\left|(T(t) - T_0)/T(t)\right|$. The results are shown in Fig 5 a), where Er is plotted as a function of the time. It should be noted that, although this error increases slightly with time, at t = 200 s it is less than 1 % and consequently the temperature T(t) can be regarded as approximately constant. In this sense, one remarkable theoretical aspect of our device is that it does not incorporate any control system to maintain the gas temperature almost constant. On the other hand, Fig 5 b) depicts the heat capacities $c_p(t)$ and $c_v(t)$ as functions of the time taking into account Eqs (20) and (21) for all temperatures T(t), which are close to the input temperatures as shown in Fig 5 a).

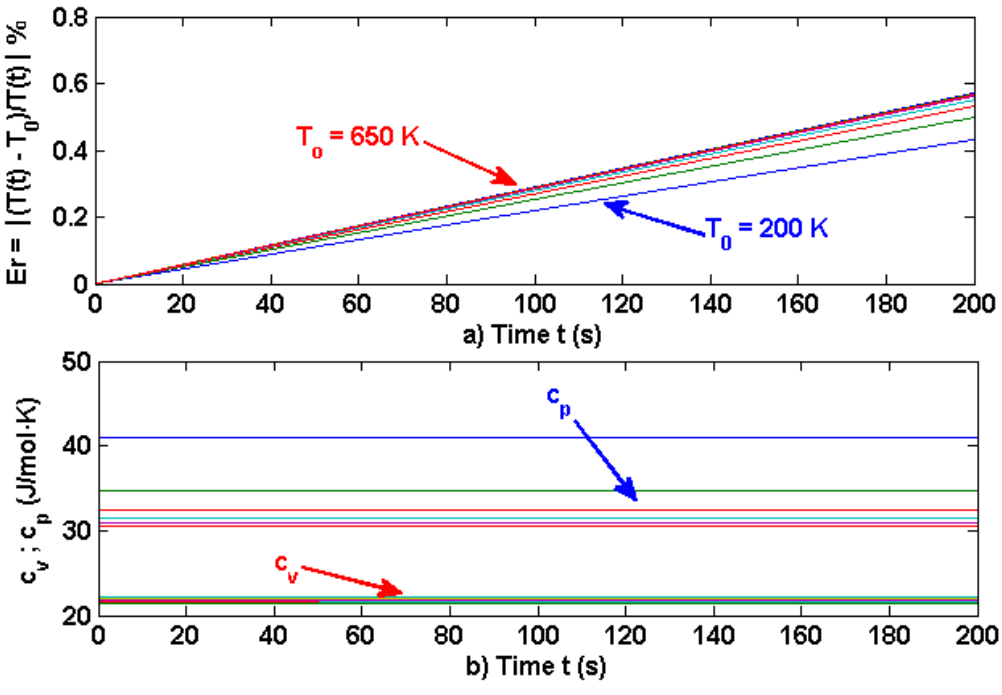

Fig. 5 Relative error (%) between the gas temperatures T(t) and the input temperatures T_0 as a function of the time. b) Heat capacities c_p and c_v as functions of the time for each gas temperature T(t).

Fig 6 shows three strange attractors in the phase plane defined by the state variables $x_1(t)$-$x_2(t)$ for the temperatures T_0 = *[200, 400, 650]* K, which provides reasonable evidence that the oscillations shown in Figs 4 a) and b) are chaotic.

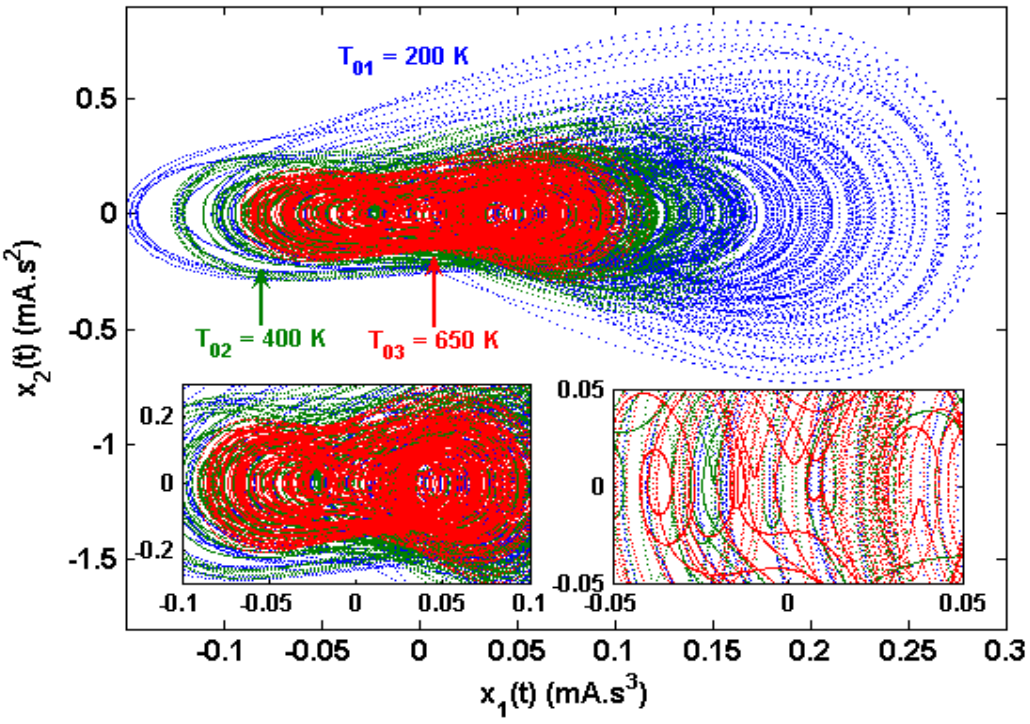

Fig. 6 Strange attractors in the phase plane $x_1(t)$-$x_2(t)$ for three temperatures T_{01}, T_{02} and T_{03} corresponding to the simulation parameters indicated at the legend of Fig 4.

The previous calculations have also been carried out for the argon [23] by using the same parameters of Fig 4 in a wide range of temperatures. Like in the case of nitrogen, the results indicate chaotic regime and are in good agreement with the experimental data as can be observed in Figs 7 a) and b). On the other hand, in Fig 7 c) the second virial coefficient is plotted for several gases by using the dimensionless coordinates:

$$T^* = \frac{k_B T}{\varepsilon_p} \;\; ; \;\; B^* = \frac{B}{b_{0v}} \;\; ; \;\; b_{0v} = \frac{2\pi}{3} N_A \sigma_p^3 \tag{28}$$

where k_B is the Boltzmann constant, N_A is the Avogadro number and ε_p, σ_p are parameters of the inter-molecular Lennard-Jones potential tabulated for each gas [15] [24]. The estimated data for the argon obtained from chaotic oscillations are close to the experimental data, which is another clear verification that the outlined procedure works reasonably well for the virial coefficient estimation.

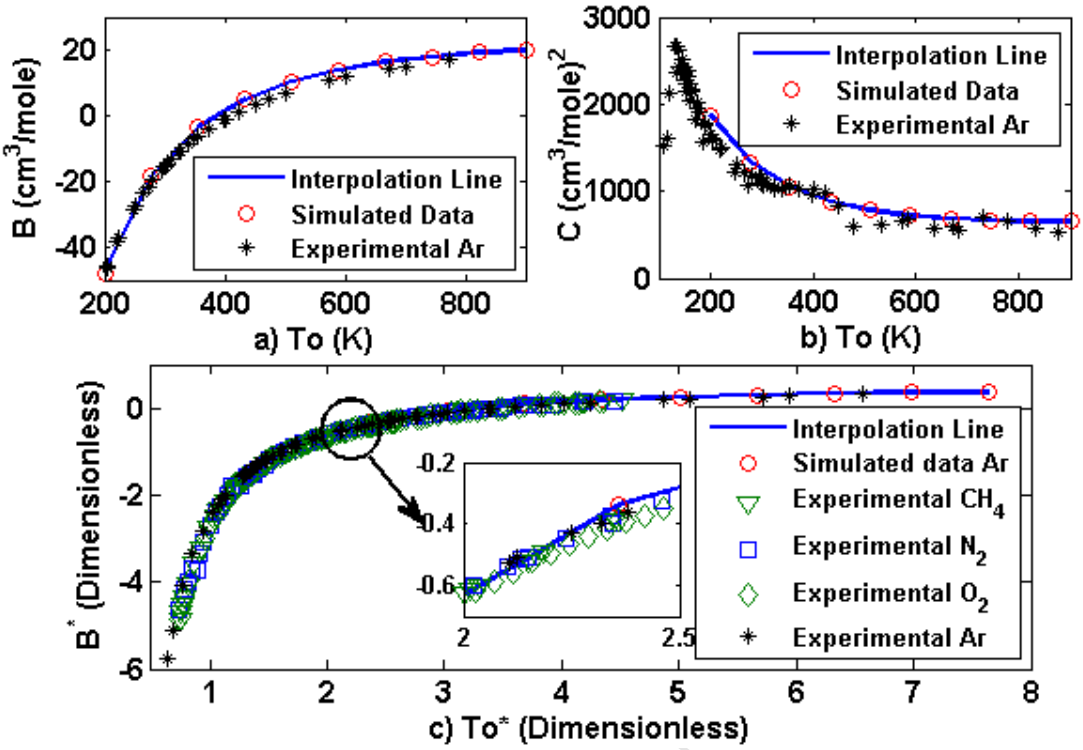

Fig. 7 a) Experimental and simulated data for the second virial coefficient *B* of the argon as a function of the temperature, obtained from chaotic behavior. b) Experimental and simulated data for the third virial coefficient *C* of the argon as a function of the temperature, obtained from chaotic behavior. c) Dimensionless experimental and simulated data for the virial coefficient *B* of the argon as a function of the dimensionless temperature obtained from chaotic behavior. A comparison with the corresponding data for the methane, oxygen and nitrogen is also shown.

In view of the results shown in Figs 2 to 7, it should be remarked that the concordance between the theoretical and experimental virial coefficients B and C requires two conditions: i) An empirical equation of state which describes suitably the behavior of the considered gas at low and high pressures. ii) Enough variability in the simulation data to capture the gas properties, which in turn allows to estimate the virial coefficients B and C through Eq (23). Such variability in the simulation data is achieved by means of the chaotic behavior, which is obtained taking parameter values which give self-oscillating behavior (see Eqs 15-17) and varying harmonically the time constant of the pressure probe (Eq (27)). Consequently, although there is nothing random in the system Eqs (11), the system behavior becomes unpredictable.

On the other hand, the thermodynamic equilibrium of the system is reached when the following condition is verified [25]:

$$F_1 \cdot F_2 \cdot F_3 = \left(\frac{\partial v}{\partial T}\right)_P \left(\frac{\partial P}{\partial v}\right)_T \left(\frac{\partial T}{\partial P}\right)_v = -1 \qquad (29)$$

To verify that equation (29) holds, in Fig 8 d) the product $F_1 \cdot F_2 \cdot F_3$ is been plotted as a function of the time taking into account the SRK state equation, which allows to observe that it is exactly fulfilled that $F_1 \cdot F_2 \cdot F_3$ = -1. Additionally, F_1, F_2 and F_3 are plotted separately in Figs 8 a), b) and c) to show that their values are quite far from unity, which however does not contradict that their product is exactly equal to -1. The same conclusion is reached for the equations of state indicated in the Appendix as well as for the high precision equations of state that will be considered in the next section.

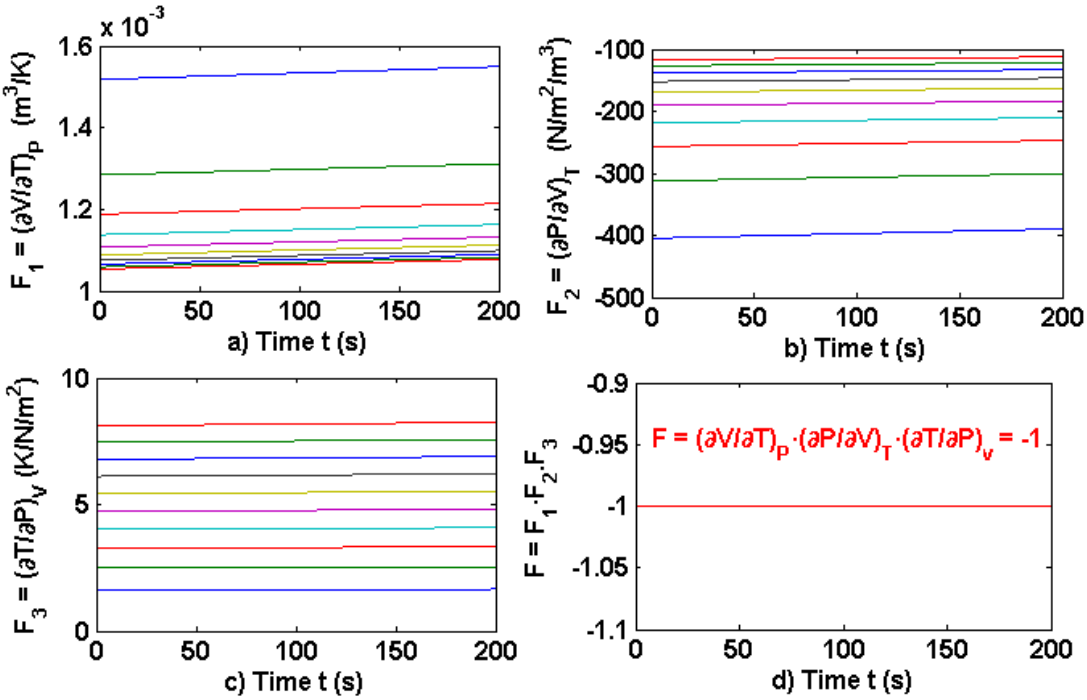

Fig. 8 a) Variation of $\left(\partial v/\partial T\right)_P$ as a function of the input temperature T_0 and the time. b) Variation of $\left(\partial P/\partial v\right)_T$ as a function of the input temperature T_0 and the time. c) Variation of $\left(\partial P/\partial T\right)_v$ as a function of the input temperature T_0 and the time. d) Variation of $\left(\partial v/\partial T\right)_P \cdot \left(\partial P/\partial v\right)_T \cdot \left(\partial T/\partial P\right)_v$ as function of the input temperature T_0 and time.

4. Application for non-polar and polar gases with high precision equations of state

In this section we shall describe how the virial coefficients can be estimated for polar gases as well as for a mixture of non-polar gases by using high precision equations of state.

4.1 Estimation of second virial coefficient for dry air

The results obtained in the previous section suggest that the theoretical device considered in this paper could be used for estimating the second virial coefficient of a mixture of real gases, such as the dry air. For this purpose, we use Eq (23) assuming that the pressures are sufficiently small so that the effect of the virial coefficients *C(T)*, *D(T)* and so on is negligible. The used procedure is summarized through the following steps:

a) We establish a set of gas inlet temperatures T_0, which are the temperatures for which the viral coefficient *B(T)* is estimated.

b) We use an empirical state equation of high precision defined as a function of the molar Hemlholtz energy, which is decomposed into a term representing the ideal gas behavior and a residual term due to the gas non-ideality [9], i.e.:

$$\frac{a(T,\rho)}{RT}=\frac{a^{id}(T,\rho)+a^{R}(T,\rho)}{RT}=\alpha^{id}(T,\rho)+\alpha^{R}(T,\rho) \tag{30}$$

where the superscripts *id* and *R* refer to the ideal and residual terms respectively. The ideal term is defined as:

$$\alpha^{id}(T,\rho)=\frac{1}{RT}\int_{T^*}^{T}c_v^{id}(T)\,dT-\frac{1}{R}\int_{T^*}^{T}c_v^{id}(T)\frac{dT}{T}+\ln\frac{\rho}{\rho_0}+\frac{a(T^*,\rho^*)}{RT} \tag{31}$$

where T^* and ρ^* are small reference values for which the gas behavior can be regarded as ideal, and $c_v^{id}(T)$ is the specific heat of the gas at constant volume. The equation of state for the real gas is expressed as:

$$P(T,\rho)=-\left(\frac{\partial a(T,\rho)}{\partial v}\right)_T \;;\; P(T,\rho)=\rho RT\left[1+\delta\left(\frac{\partial\alpha^{R}(\tau,\delta)}{\partial\delta}\right)_\tau\right] \;;\; \delta=\frac{\rho}{\rho_c} \;;\; \tau=\frac{T_c}{T}$$

$$\alpha^{R}(\tau,\delta)=n_1\delta\tau^{0.25}+n_2\delta\tau^{1.125}+n_3\delta\tau^{1.5}+n_4\delta^2\tau^{1.375}+n_5\delta^3\tau^{0.25}+$$
$$n_6\delta^7\tau^{0.875}+n_7\delta^2\tau^{0.625}\exp(-\delta)+n_8\delta^5\tau^{1.75}\exp(-\delta)+n_9\delta\tau^{3.625}\exp(-\delta^2)+$$
$$n_{10}\delta^4\tau^{3.625}\exp(-\delta^2)+n_{11}\delta^3\tau^{14.5}\exp(-\delta^3)+n_{12}\delta^4\tau^{12}\exp(-\delta^3) \tag{32}$$

where ρ_c and T_c are the critical density and the critical temperature respectively, whereas the coefficients n_i *(i=1,...,12)* can be found in Ref [9] for several non-polar gases. As we shall see later, Eq (32) provides with a great precision in the estimation of *B(T)*. The relation between *P(t)* and $\rho(t)$ (see Fig 1 and Eqs (6)) is given for each temperature T_0, whereas the value of $\rho_2(t)$ is obtained iteratively in each simulation step from the values of $P_2(t)$ and T_0 by means of Eq (32). In the case of polar gases, a similar equation to Eq (32) will be considered as shown in Refs [8,9].

c) As previously indicated, the application of the model to obtain theoretically the second virial coefficient requires maintaining the vessel gas temperature approximately constant (see Figs 1 and 2). For this purpose, we assume a vessel volume of 1 m^3, for which according to Eqs (5)-(7) the density and the temperature of the gas will remain approximately constant.

d) The chaotic behavior is necessary to assure a high variability in the simulation data at each temperature T_0, so that the polynomial fit of Eq (23) collects the thermodynamic properties of the gas. For this reason, it is necessary to achieve chaotic oscillations for temperatures below and above the critical one. Taking into account the analysis of section 3, we will choose suitable parameter values in Eqs (15)-(17) to obtain a self-oscillating behavior as it was discussed considering Eq (27).

e) The values for the specific heats at constant pressure (c_p) and constant volume (c_v) cannot be calculated like in the case of ideal gases (i.e. through the relation $c_p - c_v = R$). Instead, the specific heat of a particular gas at low pressure $c_p^*(T)$ can be obtained like in Eq (20), i.e. [24]:

$$c_p^*(T) = A_1 + A_2 T + A_3 T^2 + A_4 T^3 + A_5 T^4 \tag{33}$$

where T is the temperature (in *K*) and $c_p^*(T)$ is expressed with units of *J/(mole·K)*. On the other hand, since the values of $c_p^*(T)$ given in Eq (33) are determined at low pressures, it is necessary to calculate the variation of $c_p(T)$ with respect to the pressure by means of the following equation [6], [9], [25]:

$$\Delta c_p = c_p(T) - c_p^*(T) = -\int_{P_1\to 0}^{P_2} T\left(\frac{\partial^2 v}{\partial T^2}\right)_P dP \tag{34}$$

Once the specific heat at constant pressure $c_p(T)$ is known, the specific heat at constant volume $c_v(T)$ can be obtained by means of Eq (21). Taking into account Eqs (32)-(34) it is deduced that:

$$\begin{aligned} c_v(T,\rho) &= -R\tau^2\left[\left(\frac{\partial^2\alpha^{id}}{\partial\tau^2}\right)_\delta + \left(\frac{\partial^2\alpha^R(T,\rho)}{\partial\tau^2}\right)\right] \\ c_p(T,\rho) - c_v(T,\rho) &= R\frac{\left[1+\left(\frac{\partial\alpha^R(T,\rho)}{\partial\delta}\right)_\tau - \delta\tau\left(\frac{\partial^2\alpha^R(T,\rho)}{\partial\tau\partial\delta}\right)\right]^2}{\left[1+2\delta\left(\frac{\partial\alpha^R(T,\rho)}{\partial\delta}\right)_\tau - \delta^2\left(\frac{\partial^2\alpha^R(T,\rho)}{\partial\delta^2}\right)\right]} \end{aligned} \tag{35}$$

With the previous considerations, the model presented in section 2 can be applied to estimate the second virial coefficient for the dry air, which is formed by a mixture of nitrogen (non-polar, 78.1 % Vol.), oxygen (non-polar, 20.95 % Vol.), argon (non-polar, 0.9 % Vol.), carbon dioxide (non-polar, 0.03 % Vol.) and other gases in very small volumetric proportions that will not be considered in this work. Next we apply the previously described procedure for each gas individually to obtain the virial coefficients B_{ii} *(i = 1,2,3,4)* for the nitrogen, oxygen, argon and carbon dioxide. And from such virial coefficients for the individual gases, the virial coefficient $B_m(T)$ of the mixture can be obtained as [6], [9] [15-16]:

$$\begin{aligned} B_m(T) &= \sum_{i=1}^{n=4}\sum_{j=1}^{n=4} y_i y_j B_{ij}(T) \\ B_m(T) &= y_1^2 B_{11} + 2y_1y_2B_{12} + 2y_1y_3B_{13} + 2y_1y_4B_{14} + \\ & y_2^2B_{22} + 2y_2y_3B_{23} + 2y_2y_4B_{34} + y_3^2B_{33} + 2y_3y_4B_{34} + y_4^2B_{44} \end{aligned} \tag{36}$$

Since there are few experimental data for the interaction coefficients B_{ij} *(i,j = 1,2,3,4* with *i≠j)*, we shall apply an approximation based on a Lennard-Jones intermolecular potential defined as [15-16]:

$$u(r) = 4\varepsilon\left[\left(\frac{\sigma}{r}\right)^{12} - \left(\frac{\sigma}{r}\right)^{6}\right] \tag{37}$$

where r is the intermolecular distance, ε is the minimum potential energy and σ is the radius such that $u(\sigma) = 0$ when $r = \sigma$. On the other hand, the second virial coefficient of two interacting molecules can be calculated from statistical mechanics [26] as:

$$\begin{aligned} B_{ij} &= b_0^{ij} B_{ij}^* \;\; ; \;\; B_{ij}^* = -\sum_{n=0}^{\infty} \frac{2^{n-\frac{3}{2}}}{n!}\Gamma\left(\frac{2n-1}{4}\right)\left(\frac{1}{T^{\oplus}}\right)^{\frac{2n+1}{4}} \\ T^{\oplus} &= \frac{k_B T}{\varepsilon_{ij}} \;\; ; \;\; b_0^{ij} = \frac{2\pi}{3} N_A \left(10^{-8}\sigma_{ij}\right)^3 \;\; ; \;\; \varepsilon_{ij} = \sqrt{\varepsilon_i}\varepsilon_j \;\; ; \;\; \sigma_{ij} = \frac{\sigma_i + \sigma_j}{2} \end{aligned} \tag{38}$$

where Γ is the gamma function, k_B is the Boltzmann's constant, N_A is the Avogadro's number and ε_{ij} and σ_{ij} are the parameters of the Lennard-Jones potential, which are tabulated for the nitrogen, oxygen, argon and carbon dioxide [15-16]. Consequently, Eqs (36)-(38) allow to estimate the interaction virial coefficients for dry air. And the final step consists of calculating the virial coefficients for the individual gases $B_{11}(N_2)$, $B_{22}(O_2)$, $B_{33}(Ar)$ and $B_{44}(CO_2)$ as it was done in the previous section.

In Fig 9, the calculated virial coefficients for the nitrogen, oxygen, argon and carbon dioxide are plotted together with the corresponding experimental values [27]. It is interesting to highlight the good adjustment provided by the state equation of high precision given in Eq (38). Next, by applying Eqs (36)-(38) the interaction virial coefficients B_{ij} are calculated, from which the virial coefficients of dry air are obtained and shown in Fig 10. It should be noted that the temperatures are above the critical one for all gases. The parameter values are τ_i = 6 min, b_0 = 1 (1/s^3), b_1 = 0.01 (1/s^2), K_m = 3.8512·10^{10} (N/m^2)/(m^3/s), K_d = 7.5·10^{-8} (m^3/s)/(N/m^2)$^{0.5}$, K_t = 8·10^{-7} mA/(N/m^2), δ = 0.26 and ω_n = 0.69 rad/s. Moreover, the values of T_{mi} and A_{Tmi} in Eq (27) are given by:

$$\begin{aligned} T_{mi} &= \begin{bmatrix} 12.5217 & 14.1940 & 15.7319 & 17.1633 & 18.5078 \\ 19.7794 & 22.1444 & 20.9888 & 23.2528 & 24.3194 \end{bmatrix} \\ A_{Tmi} &= \begin{bmatrix} 10.4347 & 11.2058 & 11.7989 & 12.2595 & 12.6189 \\ 12.8996 & 13.1180 & 13.2867 & 13.4151 & 13.5108 \end{bmatrix} \end{aligned} \tag{39}$$

The initial conditions are defined as:

$$x_{0i} = \begin{bmatrix} x_{1e} & 0 & 0 & P_{0i} & \rho_{2i} & T_{0i} & 0 \end{bmatrix} \tag{40}$$

where $x_{1e} = x_{ei}/b_0$. It should be remarked that the last null element in Eq (40) corresponds to a new state variable $x_7(t)$ whose initial value is zero. The reason of introducing such variable relies on the fact that the time constant T_m given by Eq (27) is time dependent and therefore the system is not autonomous. Consequently, to obtain an autonomous system the variable $x_7(t)$ is defined as:

$$x_7(t) = \omega_{Tm} t \Rightarrow \frac{dx_7}{dt} = \omega_{Tm} \tag{41}$$

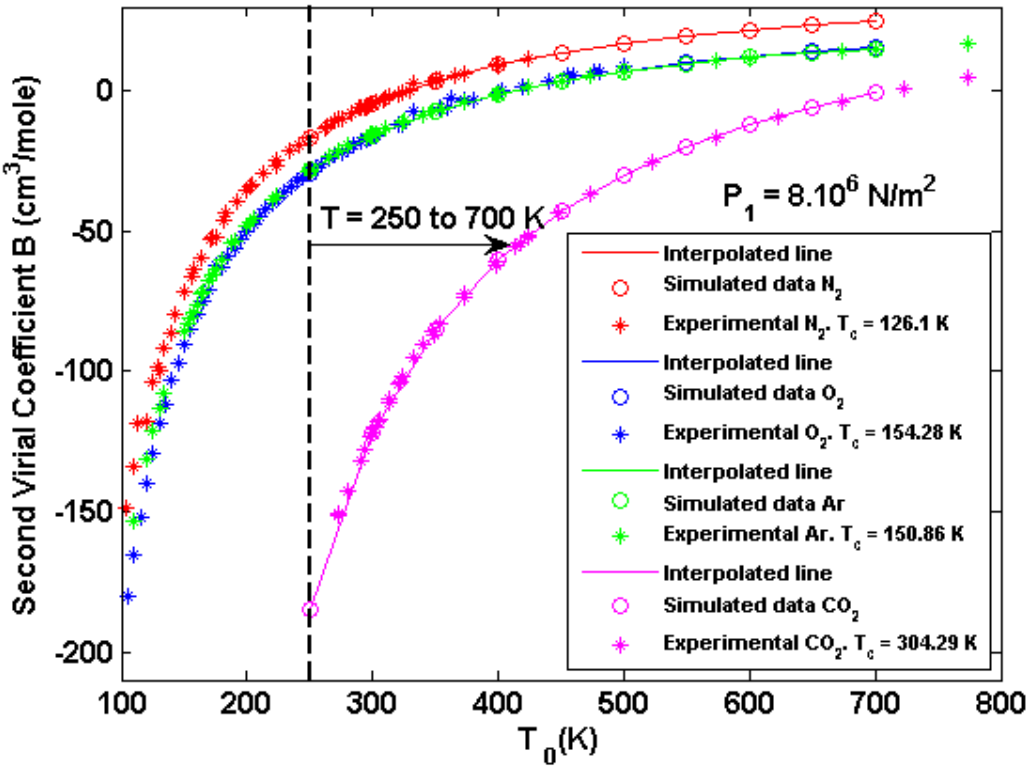

Fig. 9 Experimental and simulated data for the second virial coefficients of the nitrogen, oxygen, argon and carbon dioxide estimated for temperatures above the critical one and at a pressure $P_1 = 8 \cdot 10^6$ N/m^2.

For the sake of comparing the virial coefficients of the gas mixture and those of the individual gases, the second virial coefficients for the nitrogen and the oxygen are plotted in Fig 10. A similar procedure has been carried out for temperatures below the critical one as shown in Fig 11, with the difference that in this case the pressures must remain below the saturation pressure to avoid entering in the biphasic zone of the gases.

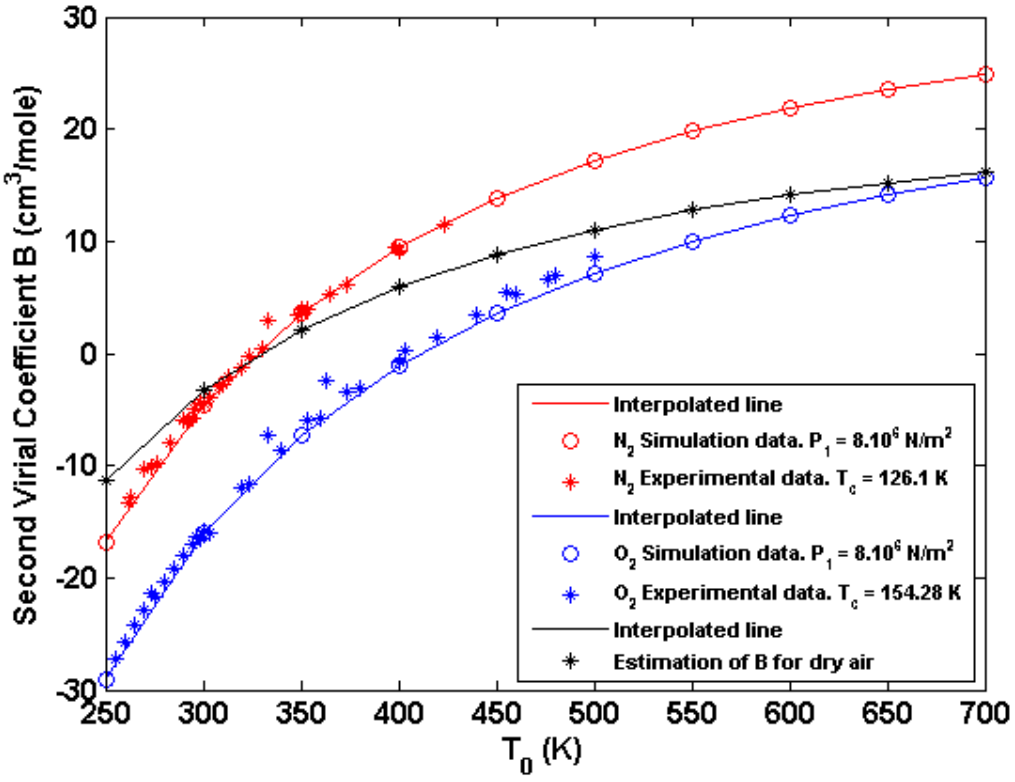

Fig. 10 Experimental and simulated data for the second virial coefficient of the nitrogen and the oxygen compared to the estimation for dry air. The temperatures and pressure are the same as in Fig 7.

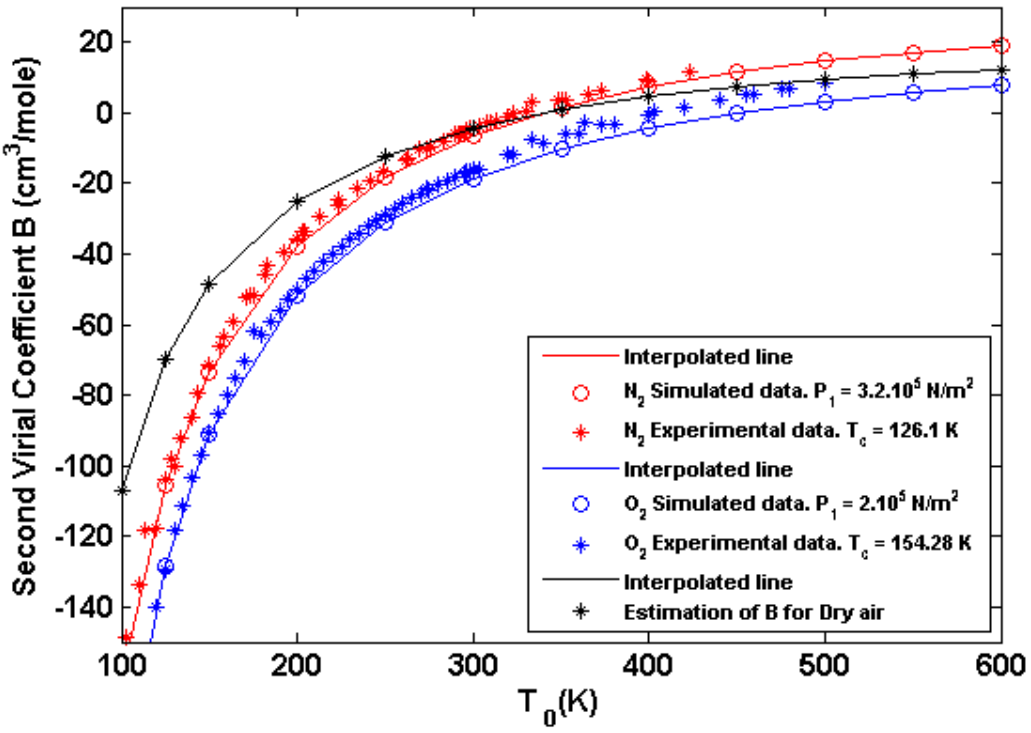

Fig. 11 Experimental and simulated data for the second virial coefficients of the nitrogen and the oxygen estimated for temperatures below the critical one and at pressures $P_1 = 3.2 \cdot 10^5$ N/m^2 (nitrogen) and $P_1 = 2 \cdot 10^5$ N/m^2 (oxygen) compared to the estimation for dry air.

The saturation pressure has been calculated by using an Antoine-type equation given by:

$$\log_{10} P^s = A + \frac{B}{T} + C\log_{10} T + DT + ET^2 \tag{42}$$

where T is expressed in K and the coefficients *A*, *B*, *C*, *D* and *E* for different gases are obtained from Ref [24]. If any of the input temperatures T_0 to the device is lower than the critical one, the value of P_1 (and $P_s < P_1$) is taken lower than the saturation pressure P^s so that the chaotic pressure oscillations are smaller than the saturation pressure P^s.

4.2 Extension to polar gases

To demonstrate that our methodology works properly for polar gases, we will also analyze the ammonia for which it is possible to estimate the virial coefficients. For this purpose, the following high precision equation of state shall be applied:

$$P(T,\rho) = -\left(\frac{\partial a(T,\rho)}{\partial v}\right)_T$$

$$P(T,\rho) - \rho RT\left[1 + \delta\left(\frac{\partial \alpha^R(\tau,\delta)}{\partial \delta}\right)_\tau\right] = 0 \;\; ; \;\; \delta = \frac{\rho}{\rho_c} \;\; ; \;\; \tau = \frac{T_c}{T}$$

$$\alpha^R(\tau,\delta) = n_1\delta\tau^{0.25} + n_2\delta\tau^{1.25} + n_3\delta\tau^{1.5} + n_4\delta^3\tau^{0.25} + n_5\delta^7\tau^{0.875} + \tag{43}$$

$$n_6\delta\tau^{2.375}\exp(-\delta) + n_7\delta^2\tau^2\exp(-\delta) + n_8\delta^5\tau^{2.125}\exp(-\delta) + n_9\delta\tau^{3.5}\exp(-\delta^2)$$

$$+ n_{10}\delta\tau^{6.5}\exp(-\delta^2) + n_{11}\delta^4\tau^{4.75}\exp(-\delta^2) + n_{12}\delta^2\tau^{12.5}\exp(-\delta^3)$$

Eq (43) is very similar to Eq (32) and it will be applied to the ammonia following the simulation steps discussed in subsection 4.1. Fig 12 shows the simulation results for the ammonia considering two cases. In the first case, the minimum temperature is below the critical one, i.e. T_{0min} = 325 K < T_c = 405.65 K, and the corresponding saturation pressure given by Eq (42) is $P^s = 3.8647\cdot 10^6$ N/m^2. Consequently, to avoid entering the biphasic zone of the NH_3, the input gas pressure is set to $P_1 = 3\cdot 10^6$ N/m^2 < P^s. It can be observed that the values of virial coefficient B in Fig 11 a) are in good agreement with the experimental data, although the adjustment of virial coefficient C to the experimental data is poor as shown in Fig 12 b). This is due to

the fact that, at low pressures, only coefficient B is relevant in the virial expansion. In the second case, the minimum temperature is T_{0min} = 425 K > T_c and the value of the initial pressure is taken as $P_1 = 9 \cdot 10^6$ N/m^2. Like in the first case, in Figs 12 c) and d) we can observe that the virial coefficient B is in good agreement with the experimental values, but now the fitting of the virial coefficient C to the experimental data is significantly better. This result is expectable due to the fact both B and C are relevant in the virial expansion at high pressures.

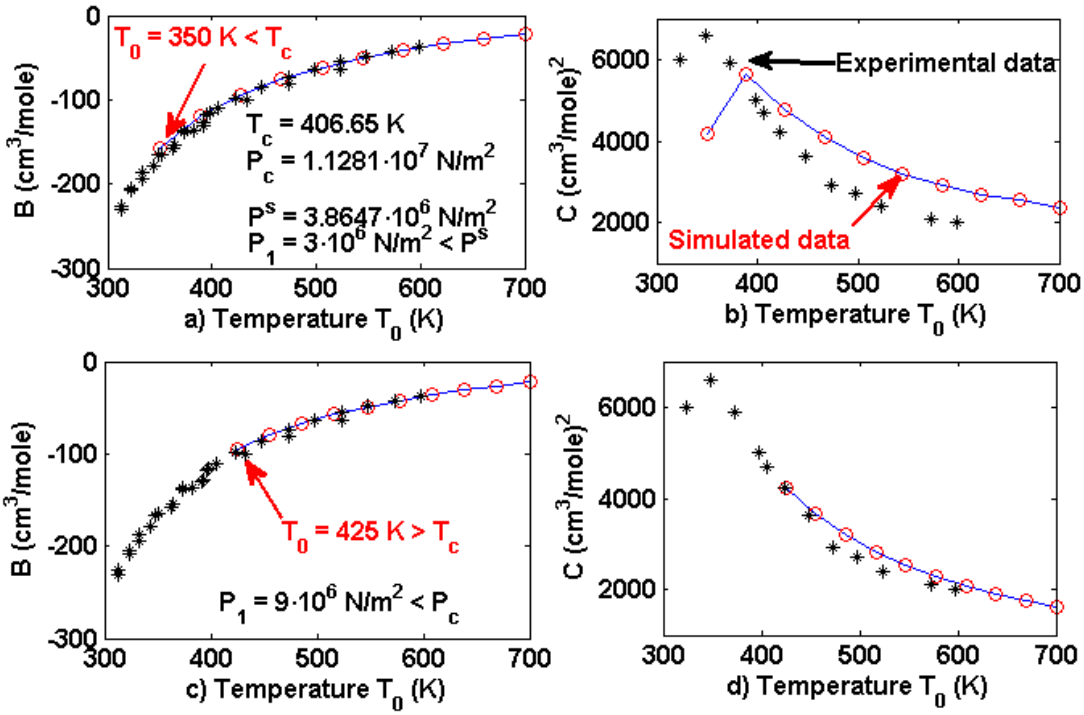

Fig. 12 Experimental and simulated values of the viral coefficients B and C obtained with the high precision equation of state for the ammonia. a) Virial coefficient B for $P_1 < P^s$. b) Virial coefficient C for $P_1 < P^s$. c) Virial coefficient B for $P_1 > P^s$. d) Virial coefficient C for $P_1 > P^s$.

To conclude this section, figure 13 illustrates a flowchart which summarizes the required steps to estimate the virial coefficients of a real gas in accordance with the previously described methodology. It should be noticed that to obtain chaotic oscillations it is necessary to assure self-oscillating behaviour by choosing adequate values for δ, ω_n, K_{NL} and τ_i as well as to include an adequate external harmonic disturbance given by Eq (27).

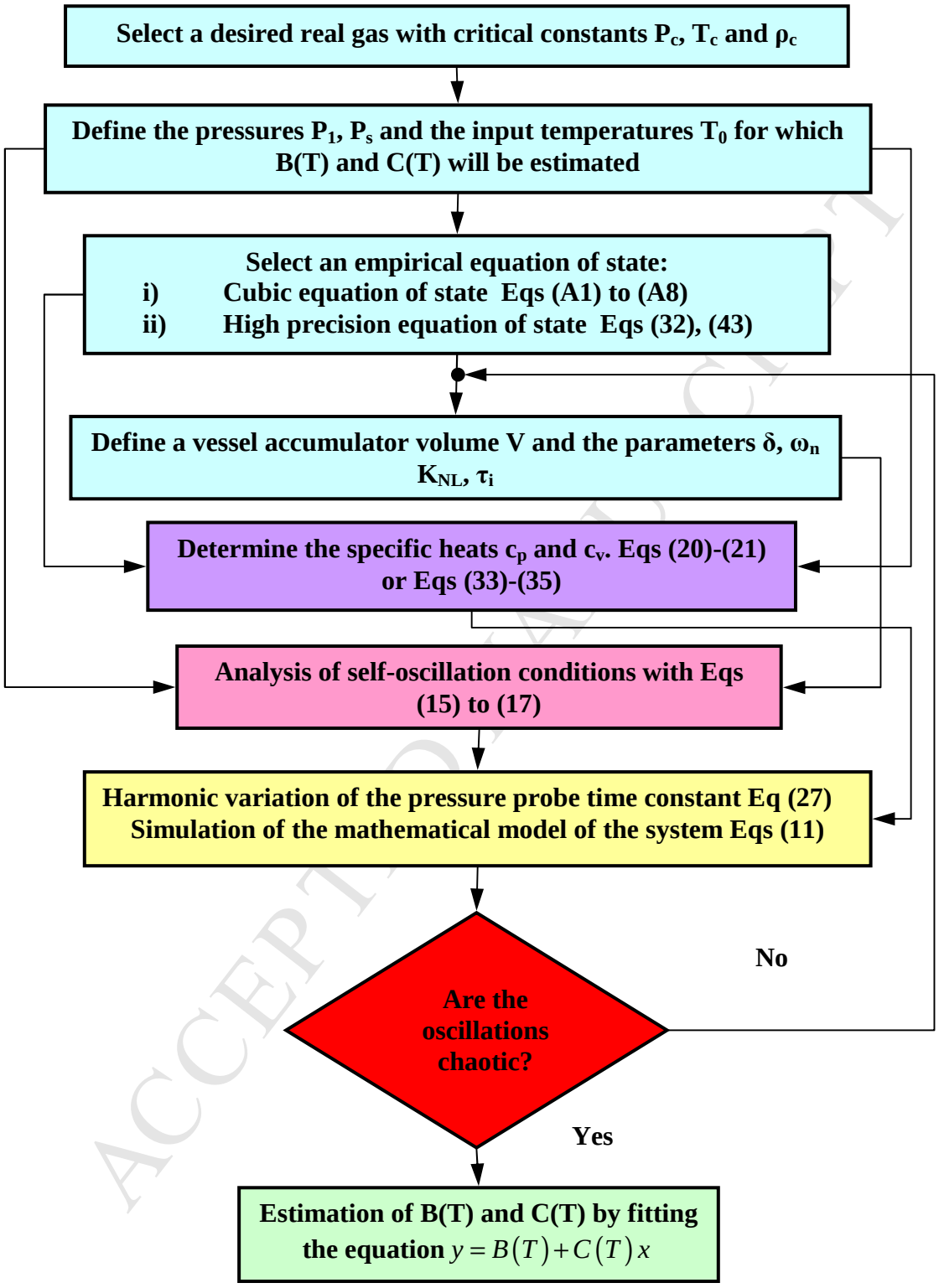

Fig. 13 Flowchart for the estimation of the virial coefficients B(T) and C(T).

5. Application to quantum gases

In this section we shall apply the results of the sections 3 and 4 to the following quantum gases: Helium 4, Helium 3, Hydrogen, Deuterium and Neon. The Tritium will not be considered here since there are not experimental data for the virial coefficients [27-29]. The main difficulty that arises from working with quantum gases is that, in general, the cubic equations of state cannot be used thus becoming necessary to apply an individualized equation of state for each gas. Such individualized equations can be very complicated with many parameters such as in the case of He4 [30] or H_2 [31], whereas other equations are based on Quantum Mechanics like in the cases of H_2 and D_2 [32]. On the other hand, the Helmholtz potential function by using the Debye function for He3 [33] and the radial distribution function with quantum corrections for the Ne [34-35] have been also developed as alternative approaches.

The application of the aforementioned individual equations of state in the context of the system presented in this paper may become very complicated. In fact, it should be noted that it is necessary to reach chaotic oscillations in wide ranges of pressure and temperature to obtain acceptable values for the virial coefficients B and C. For this reason, we have used several cubic equations of state whose unified form appears in Eq (18) (see Appendix). A detailed analysis of the capabilities of such cubic equation is reported in Refs [20] and [36].

In all cubic equations of state, the parameters *a* and *b* depend on the critical temperature T_c and critical pressure P_c, which in the case of quantum gases (i.e. molecules of low molecular weight whose properties are more accurately described by means of Quantum Mechanics) must be substituted by the effective critical constants defined by the empirical relations given by [16], [28]:

$$T_c = \frac{T_c^0}{1+\dfrac{21.8}{M \cdot T}} \quad ; \quad P_c = \frac{P_c^0}{1+\dfrac{44.2}{M \cdot T}} \tag{44}$$

where M is the molecular mass (gr/mol) and T is the temperature expressed in K, whereas $T_c^{\,0}$ and $P_c^{\,0}$ are the so called classical critical constants, which are tabulated for

the quantum gases. Eqs (44) must be applied taking the acentric factor $\omega = 0$ (see the Appendix). It should be pointed out that the corrections given by Eqs (44) are more significant at low temperatures, since when $T \to \infty \Rightarrow T_c \to T_c^0$; $P_c \to P_c^0$. Consequently, T_c and P_c are approximately constant at high temperatures.

The simulation results obtained with cubic equations and Eqs (44) provide simulation results which even in chaotic regime completely disagree with the experimental data for the virial coefficients B and C of all quantum gases [29]. To overcome this problem, we have introduced another empirical modification of Eqs (44), which consists of introducing a temperature dependent function so that the modified values of T_c and P_c are written as:

$$T_{cm} = \frac{T_c^0}{1+\dfrac{21.8}{f_M M \cdot T}}\left[\frac{1+\dfrac{1}{F_v(T)}}{1+\dfrac{1}{F_v(T_1)}}\right] \;\; ; \;\; P_{cm} = \frac{f_P P_c^0}{1+\dfrac{44.2}{f_M M \cdot T}} \qquad (45)$$

$$F_v(T) = fFv + (1-fFv)\left(1-\exp\left(-feFv\left(\frac{T-T_1}{T_{\max}-T_1}\right)\right)\right) \;\; ; \;\; F_v(T_1) = fFv$$

where T_{cm} and P_{cm} are the modified critical constants and f_M, f_P, fFv and $feFv$ are adjustable parameters, whereas T_1 and T_{max} are respectively the lowest and highest temperature from which the virial coefficients B and C are estimated through the simulation data. It should be noted that if $fFv = 1$ then $F_v(T) = 1$.

Once the virial coefficients are estimated by using a cubic equation of state in accordance with Eqs (45), it is possible to approximate the intermolecular potential. For this purpose, we assume a Mie-type intermolecular potential [16] written as:

$$u(T,r) = f_0(T)\left[\frac{n(T)}{6}\right]^{\frac{6}{n(T)-6}} \frac{n(T)}{n(T)-6}\varepsilon\left[\left(\frac{\sigma}{r}\right)^{n(T)} - \left(\frac{\sigma}{r}\right)^6\right] \qquad (46)$$

where in case that *n* depends on the temperature and $f_0(T) = 1$ for $n(T) = 12$, Eq (44) provides the Lennard-Jones intermolecular potential of Eq (37). Nevertheless, the function $f_0(T)$ is an empirical factor that takes the form:

$$f_0(T) = \frac{1}{F_v(T)} = \frac{1}{fFv + (1 - fFv)\left(1 - \exp\left[-feFv(T - T_1)/(T_{\max} - T1)\right]\right)} \tag{47}$$

where $f_0(T) = 1$ if $fFv = 1$. On the other hand, it should be recalled that the radial distribution function (i.e. the local densities at various distances from a particular molecule divided by the bulk average density of the gas) can be expressed as [26]:

$$g(r, \rho, T) = \exp\left[u(T, r)/k_B T\right]\left[1 + \rho g_1(r, T) + \rho^2 g_2(r, T) + ...\right] \tag{48}$$

where $u(T,r)$ is an intermolecular potential which can be defined by Eq (46). On the other hand, the state equation can be expressed as a function of the radial distribution function in the form:

$$\frac{Pv}{N_A k_B T} = 1 - \frac{2\pi\rho^2}{3}\int_0^\infty \frac{du(T, r)}{dr} g(r, \rho, T) r^3 dr \tag{49}$$

Substituting Eq (48) into Eq (49) and considering the radial distribution function up to first order approximation, the second virial coefficient *B* can be written as [26]:

$$B(T, n) = N_A\left(\frac{-2\pi}{3k_B T}\right) f_0(T)\int_0^\infty \frac{du(r, T)}{dr}\exp\left[\frac{-u(r, T)}{k_B T}\right] r^3 dr \tag{50}$$

The radial distribution function can be estimated from the empirical function $f_0(T)$, which will allow to elucidate to what extent the modified cubic state equations (18) and (45) can provide an accurate second virial coefficient. This aspect will be discussed in detail with the Helium 4, and the obtained conclusions will be applied to the rest of quantum gases.

It should be remarked that from Eqs (46)-(48) it is possible to estimate several values of B by assuming a set of values for *n* at a given temperature *T*. Among such values for *n*, the one that is chosen will be that which provides the closest value of B to the value estimated from the chaotic data. Next we shall analyze how to obtain the virial coefficients for quantum gases by using Eqs (44)-(48).

5.1 Helium 4

In the case of Helium 4 (He 4) we consider twenty-four values for the temperatures T_0 between *45* and *800* K as well as $P_1 = 10$ MPa and $P_s = 7$ MPa (both of them above the critical pressure). Taking into account Eqs (11) we choose $\delta = 0.26$, $\omega_n = 0.69$ rad/s, $b_0 = 3$ $mA^{-1}\cdot s^{-3}$ and $b_1 = 0.03$ $mA^{-1}\cdot s^{-2}$, for which the values of K_{NL} for self-oscillating behavior are obtained when the conditions given by Eqs (15)-(17) are fulfilled. Therefore twenty-four values for K_{NL} ranging between $1.25\cdot10^5$ and $1.3341\cdot10^7$ s^{-6} are obtained.

Once the self-oscillating behavior has been obtained we assume that the time constant T_m of the pressure probe (see Eqs (11)) is varied harmonically as shown in Eq (27) taking $\omega_{Tm} = 0.8$ rad/s, twenty four values for T_{mv} between *5* and *10* s and other twenty four values for A_{Tm} between *4.1667* and *5.5556* s. The simulation is carried out by using the Peng-Robinson equation of state (see Appendix) and Eqs (45) with $f_M = 15$, $f_P = 0.85$, $fFv = 0.75$ and $feFv = 4$. The simulation results are shown in Figs 10-12.

Fig 14 a) shows chaotic oscillations for the pressures P_2 for each temperature between 45 and 800 K, for which the approximately straight lines represent the choked pressures. Fig 14 b) shows the chaotic oscillations of ρ_2 (for comparison see Figs 2 a)-b) and 4 a)-b)). In Fig 14 c) the vessel temperatures are plotted showing nearly straight lines, in accordance with the fact that the gas temperature is nearly constant. Furthermore, the chaotic behavior can also be appreciated in Fig 14 d), which shows a strange attractor obtained by using the auxiliary variables $x_1(t)$ and $x_2(t)$ defined in Eq (1) for a gas temperature of 100 K. Similar graphics can be obtained for the rest of temperatures between 45 and 800 K.

In Fig 15, the estimation of the virial coefficients is compared with the experimental data. The error in the experimental data for coefficient B is ± 1 cm^3/mol, so the estimation from the simulated data can be regarded as acceptable. The experimental values of C can be inaccurate depending on the used experimental procedure. However, it is clear that the estimation of C for the He4 could only be used within the temperature range between 45 and 200 K.

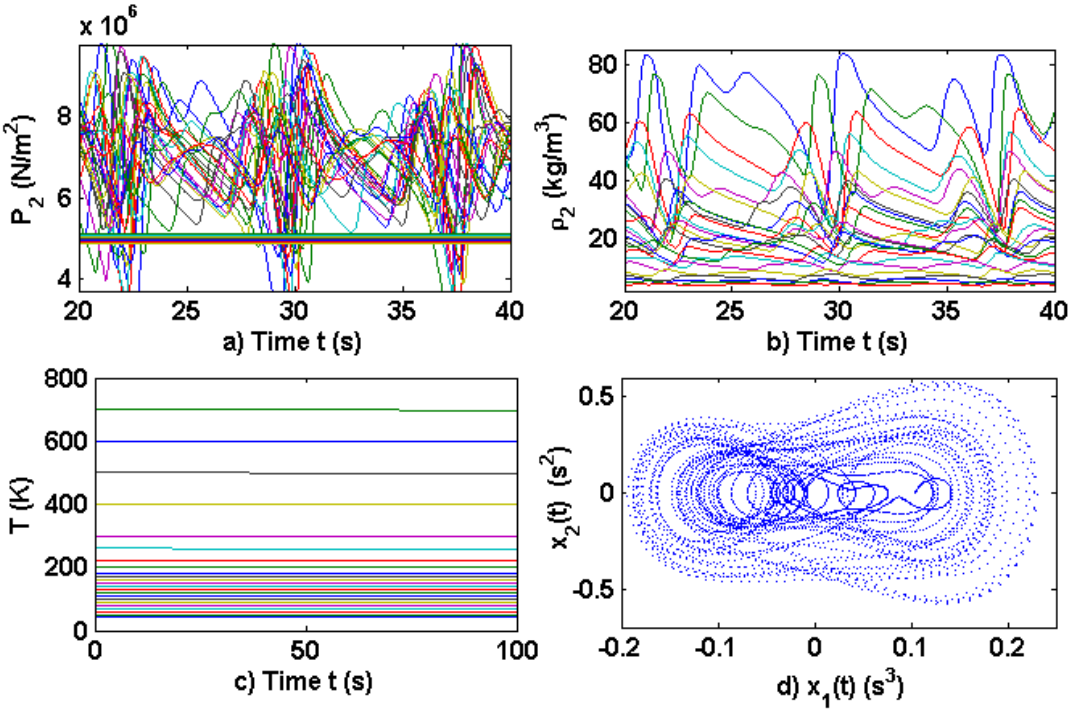

Fig. 14 a) Chaotic oscillations in the pressure $P_2(t)$ measured by the pressure probe for the Helium 4, for which the choked pressures are the approximately straight lines. b) Chaotic oscillations in the density $\rho_2(t)$. c) Approximately constant temperatures $T_{vi}(t)$ of the gas in the vessel. d) Strange attractor in the phase plane $x_1(t)$-$x_2(t)$.

Fig 16 a) shows simulation data for the second virial coefficient and the exponent *n* of the intermolecular potential given by Eqs (46) and (47). The mean value of *n* is 11.4995, which is in agreement with a Lennard-Jones intermolecular potential as shown in Eq (37). Fig 16 b) shows the radial distribution function assuming $n = 12$ and $fFv = 1$ in Eq (47) (i.e. with $f_0(T) \equiv 1$ for several temperatures). In Fig 16 c), the radial distribution function is also plotted but now taking $fFv = 0.75$ and $feFv = 4$ in Eq (47), which are used in the simulation to estimate the coefficients B and C of Fig 14. In Fig 16 d), the second virial coefficient B is calculated from Eq (48) taking $f_0(T) = 1$ (B_{21}) and $f_0(T) \neq 1$ (B_{22}). It should be noted that the values of B_{22} are close to those obtained from the chaotic oscillations depicted Fig 13 a), in accordance with the empirical equations (45) and (47).

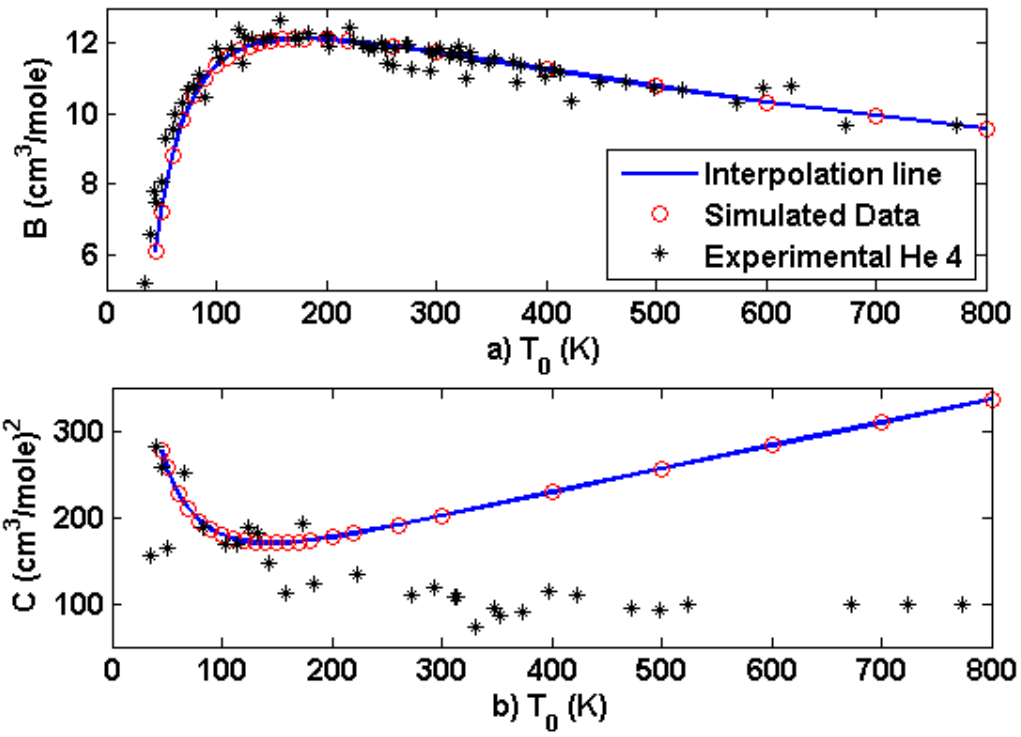

Fig. 15 a) Experimental and estimated values for the second virial coefficient B for Helium 4. b) Experimental and estimated values for the third virial coefficient C for Helium 4.

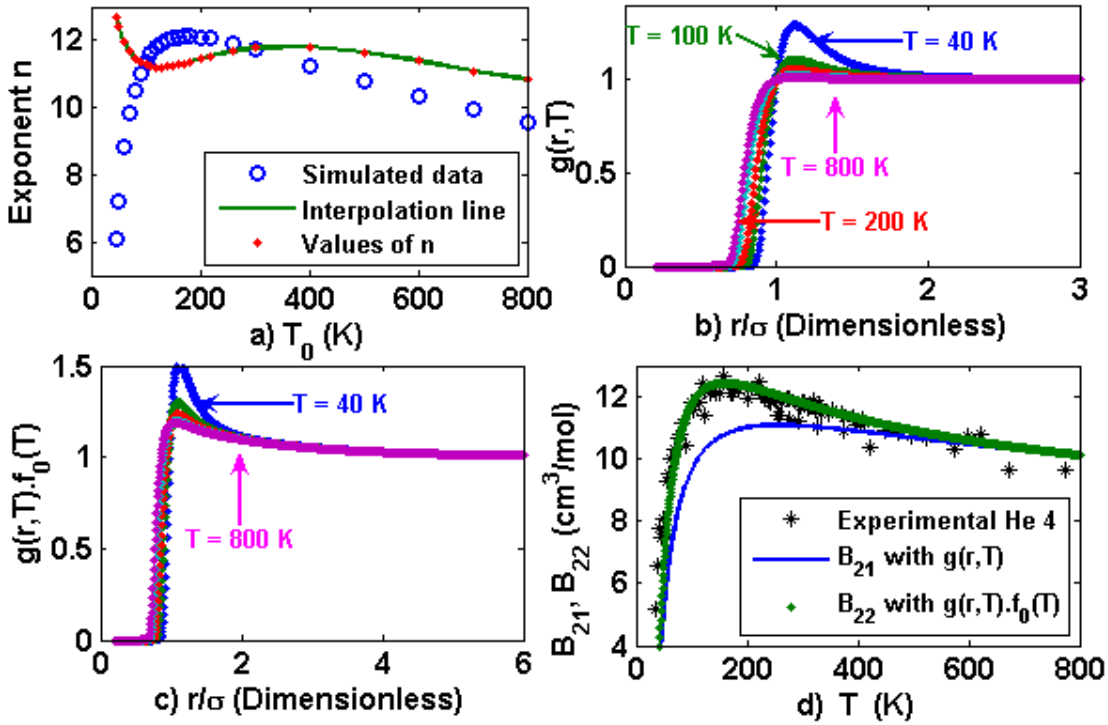

Fig. 16 a) Simulation data to obtain the virial coefficient B for Helium 4 and estimated values of exponent *n* for the intermolecular potential given by Eq (44). b) Radial distribution function for Helium 4 assuming that $f_0(T)= 1$ and a mean value of $n = 12$ (Lennard-Jones potential). c) Radial distribution function for Helium 4 with $n =12$ and $f_0(T) \neq 1$. d) Values of the second virial coefficients: B_{21} is calculated by using $n = 12$ and $g(r,T)$, whereas B_{22} is obtained by using $n = 12$ and $g(r,T)f_0(T)$.

Next we shall investigate if the other cubic equations of state could be used to estimate the virial coefficients for Helium 4. The simulation results show that by using any of the equations of state indicated in Appendix 1, the results are very different to the ones shown in Fig 15. To analyze this issue, the generalized equation of state given by Eq (18) is expanded into powers of v^{-1}, i.e.:

$$z=\frac{Pv}{RT}=\frac{v}{v-b}-\frac{\left[\Theta(T)/RT\right]v(v-\eta)}{(v-b)\left(v^2+\delta_1 v+\varepsilon\right)}=1+\left(b-\frac{\Theta(T)}{RT}\right)\frac{1}{v}+\left[(\eta+\delta_1-b)\frac{\Theta(T)}{RT}+b^2\right]\frac{1}{v^2}+\ldots$$

$$B=b-\frac{a\alpha(T_r)}{RT}\ ;\ C=(\eta+\delta_1-b)\frac{a\alpha(T_r)}{RT}+b^2 \qquad (51)$$

Consequently, in principle it is possible to obtain the virial coefficients B and C as indicated in Eqs (51). Since the PR equation of state is in reasonable agreement with the experimental values, we can take this equation as reference and adjust the values of *a* and *b* in the rest of equations of state shown in the Appendix so that they coincide with the values of *a* and *b* given in Eq (A3). To detail the proposed procedure, it is assumed that the values of *a* and *b* of the SRK equation of state shall be modified. For this purpose, the value of *b* is denoted through the subscript PR or SRK as follows:

$$b_{PR}=0.0778\frac{RT_{cm}}{P_{cmPR}}=K_{bPR}\frac{RT_{cm}}{P_{cmPR}}\ ;\ b_{SRK}=0.08664\frac{RT_{cm}}{P_{cmSRK}}=K_{bSRK}\frac{RT_{cm}}{P_{cmSRK}}$$

$$P_{cmPR}=\frac{f_{PR}\cdot P_c^0}{1+\frac{44.2}{f_M M\cdot T}}\ ;\ P_{cmSRK}=\frac{f_{SRK}\cdot P_c^0}{1+\frac{44.2}{f_M M\cdot T}} \qquad (52)$$

It should be noted that the values of P_{cmPR} and P_{cmSRK} are denoted as P_{cm} in Eqs (45). Furthermore $f_{PR} \equiv f_P$, which is taken as $f_P = 0.85$ in the PR equation of state to obtain the simulation data of Fig 11. The value of f_{SRK} is deduced from the condition given by:

$$b_{PR}=b_{SRK}\Rightarrow\frac{K_{bPR}}{f_P}=\frac{K_{bSRK}}{f_{SRK}}\Rightarrow f_{SRK}=f_P\frac{K_{bSRK}}{K_{bPR}} \qquad (53)$$

The same procedure can be applied for the parameter *a*, i.e.:

$$a_{PR} = 0.45724\frac{(RT_{cm})^2}{P_{cmPR}} = f_{aPR}K_{aPR}\frac{(RT_{cm})^2}{P_{cmPR}} = K_{aPR}\frac{(RT_{cm})^2}{P_{cmPR}}$$
$$a_{SRK} = 0.42748\frac{(RT_{cm})^2}{P_{cmSRK}} = f_{aSRK}K_{aSRK}\frac{(RT_{cm})^2}{P_{cmSRK}} \quad (54)$$

where the value of f_{aSRK} is obtained from the condition:

$$a_{PR} = a_{SRK} \Rightarrow \frac{K_{aPR}}{P_{cmPR}} = f_{aSRK}\frac{K_{aSRK}}{P_{cmSRK}} \Rightarrow f_{aSRK} = \frac{K_{aPR}}{K_{aSRK}}\frac{f_{SRK}}{f_P} \quad (55)$$

being f_{SRK} deduced from Eq (53). In the case of the He 4 it has been corroborated that the introduction of a new coefficient f_α (between 0.4 and 0.5) multiplying $\alpha(T_r)$ in Eq (51) leads to results which are closer to the experimental values at high temperatures for all the considered equations of state. Now we shall calculate the second virial coefficient by using the equations of state shown in the Appendix taking the PR equation of state as reference. The obtained values are shown in Fig 17.

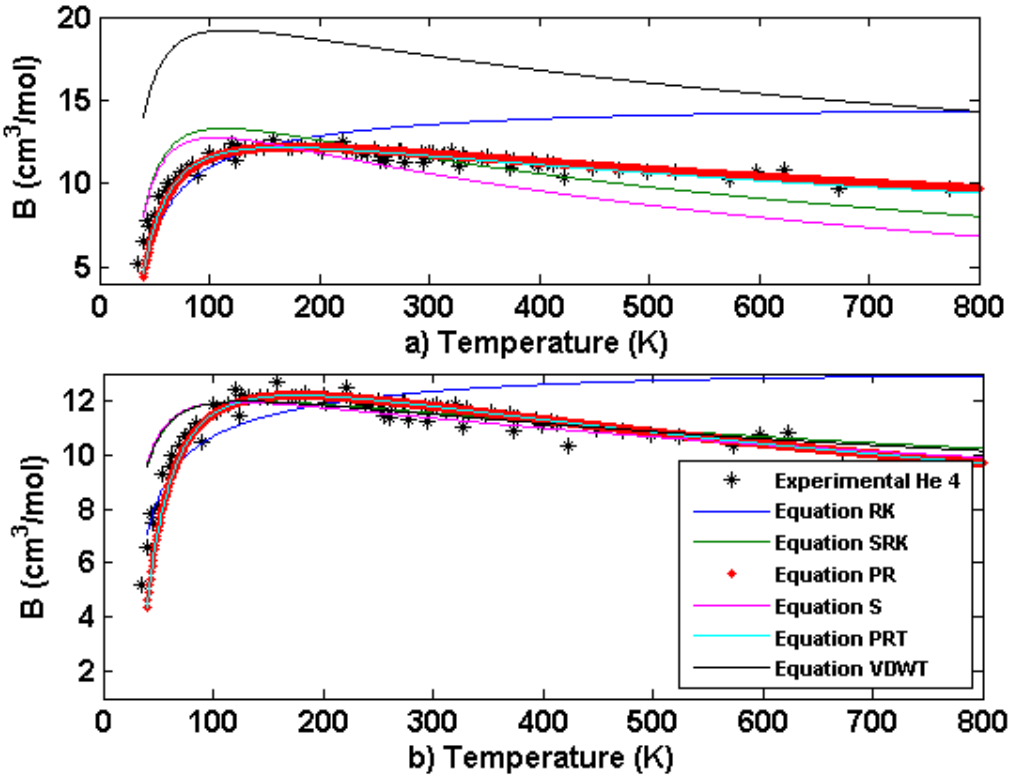

Fig. 17 Values of the second virial coefficient B obtained with the equations of state shown in the Appendix. a) Values of coefficients *a* and *b* corresponding to each of the equations of state. b) The values of *a* and *b* have been adjusted in accordance with Eqs (50)-(53) and taking $f_\alpha = 0.4$.

It should be noticed that, in Fig 17 a), only the values of B for the PR and PRT equations of state are close to the experimental values. Furthermore, the RK equation of state only provides an acceptable estimation at low temperatures, whereas the SRK equation provides a worse estimation and the VDWT equation leads to a very poor estimation. In Fig 17 b), all equations of state modified in accordance with the Eqs (52)-(55) could be used at moderate and high temperatures, and especially at low and moderate pressures for which the influence of the third virial coefficient C is not significant. It must be remarked that the previous reasoning has been made on the basis of Eqs (51) without taking into account the simulation data obtained from the chaotic oscillations, which leads to poor results for the virial coefficient C. This fact corroborates the convenience of using chaotic behavior to estimate the virial coefficients. On the other hand, table 3 shows the simulation data and parameters that have been used with all quantum gases.

TABLE 3 SIMULATION DATA AND PARAMETER VALUES FOR QUANTUM GASES

	He 4	**He 3**	**H_2**	**D_2**	**Ne**
P_c (bar)	2.28	1.17	13.13	16.64	26.53
T_c (K)	5.20	3.31	33.18	38.25	44.40
P_c^0 (bar)	6.76	6.01	20.5	20.4	27.3
T_c^0 (K)	10.47	10.55	43.6	43.6	45.5
P_1 (MPa)	10	0.18; 0.015	10	35	20
P_s (MPa)	7	0.14 ; 0.01	7	25	15
ΔT (K)	45-800	2.6-30	40-600	98-450	50-900
M (gr/mol)	4.003	3.016	2.016	4.032	20.180
f_M	15	15 ; 20	4	15	0.08
f_P	0.85	2.6 ; 3	1	1.1	0.9
fFv	0.75	1.8 ; 2	0.75	0.68	0.3
feFv	4	1.5 ; 0.5	3	5	4
n	11.4995	29.5244	30.6972	12.1814	11.0279
σ (Å)	2.551	2.56	2.827	2.982	2.82
ε/k_B (K)	10.22	10.2	59.7	37	32.6

5.2 Helium 3

The previous procedure will now be applied to Helium 3. The simulation parameters for this gas are twenty-one values for the temperatures T_0 between *5.5* and *30* K as well as $P_1 = 0.18$ MPa and $P_s = 0.14$ MPa (both of them above the critical pressure). Taking into account Eqs (11) we choose $\delta = 0.26$, $\omega_n = 0.69$ rad/s, $b_0 = 3$ $mA^{-1}\cdot s^{-3}$ and $b_1 = 0.03$ $mA^{-1}\cdot s^{-2}$. With the previous values, K_{NL} is obtained for each temperature T_0 to obtain self-oscillating behavior when the conditions given by Eqs (15)-(17) are fulfilled. Therefore we obtain twenty-one values for K_{NL} between $3.9333\cdot10^4$ and $2.9533\cdot10^4$ s^{-6} with $\tau_i = 300$ s. It is assumed that the time constant T_m of the pressure probe is varied harmonically as shown in Eq (27) taking $\omega_{Tm} = 0.8$ rad/s, twenty-one values for T_{mv} between *5 s* and *10* s and other twenty-four values for A_{Tm} between *4.1667 s* and *5.5556* s. The simulation is carried out by using the SRK equation of state (see Appendix) with a simulation step of T = 0.02 s and Eqs (45) with $f_M = 15$, $f_P = 2.6$, $fFv = 1.8$ and $feFv = 1.5$ (see table 3). The estimated values for B and C are shown in Figs 18 a) and b).

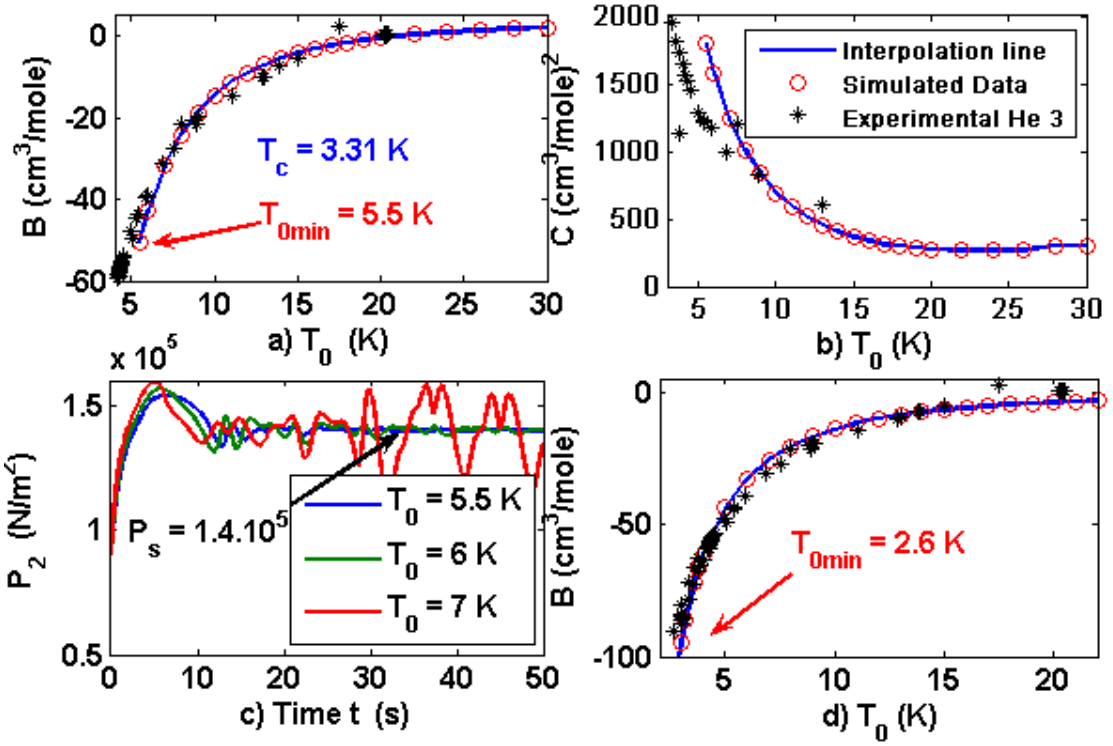

Fig. 18 Virial coefficients for the He3 using the SRK equation of state. a) Experimental and simulated values of virial coefficient B with $T_{0min} > T_c$. b) Experimental and simulated values of virial coefficient C. c) Simulated pressures P_2 for the temperatures of 5.5 K, 6 K and 7 K. The desired pressure of $1.4\cdot10^5$ N/m^2 is reached for the temperatures of 5.5 K and 6 K. d) Estimation of the second virial coefficient at low pressure (0.015 MPa) by using the PR equation of state with $T_{omin} < T_c$.

Fig 18 c) shows the pressures P_2 corresponding to the temperatures of 5.5 K, 6 K and 7 K. It should be noted that for 5.5 K and 6 K the pressures are not chaotic, and after a transient they eventually reach the desired pressure of $P_s = 1.4.10^5$ N/m^2. Consequently, the first two points of Fig 18 a) show a slightly divergent behavior respect to the experimental values. It should be recalled that this issue was discussed in the analysis of Fig 3 for self-oscillating behavior.

To verify that the proposed method can be applied to temperatures below the critical one, a new simulation has been carried out by using the PR equation of state with $f_M = 20$, $f_P = 3$, $fFv = 2$ and $feFv = 0.5$ (see Table 3). In this case, since $T_{0min} = 2.6 < Tc$, the corresponding saturation pressure has been calculated from Eq (42) and the pressure $P1 = 0.015$ MPa has been chosen below the saturation pressure to avoid entering in the biphasic zone. Due to the low pressure, the coefficient B is the dominant one in the virial expansion, whereas coefficient C and higher order virial coefficients are negligible. It should be noted that the experimental and simulated data are in reasonable agreement both for the SRK and PR equations of state. Finally, it has corroborated that similar results to the ones shown in Fig 17 are obtained for the Helium 3.

5.3 Hydrogen

The simulation data for the hydrogen consist of twenty-one values for the temperatures T_0 between *40* K and *600* K as well as $P_1 = 0.18$ MPa and $P_s = 10$ MPa (both of them above the critical pressure). Taking into account Eqs (11) we choose $\delta = 0.26$, $\omega_n = 0.69$ rad/s, $b_0 = 3$ mA$^{-1}\cdot$s^{-3} and $b_1 = 0.03$ mA$^{-1}\cdot$s^{-2}. With the previous values, K_{NL} is calculated for each temperature T_0 to obtain self-oscillating behavior when the conditions given by Eqs (15)-(17) are fulfilled. Therefore we obtain twenty-one values for K_{NL} between $1.07\cdot10^5$ and $1.8236\cdot10^5$ s^{-6} with $\tau_i = 300$ s.

Like previously considered, the time constant T_m of the pressure probe is varied harmonically as shown in Eq (27) taking $\omega_{Tm} = 0.8$ rad/s, twenty-one values for T_{mv} between *5* s and *10* s and other twenty-four values for A_{Tm} between *4.1667* s and *5.5556* s. The simulation is carried out by using the SRK equation of state (see Appendix) with a simulation step of T = 0.02 s and taking $f_M = 4$, $f_P = 1$, $fFv = 0.75$ and $feFv = 3$ in Eqs

(45) (see Table 3). Figs 19 a) and b) shows that the estimated values for B and C are both in good agreement with the experimental data.

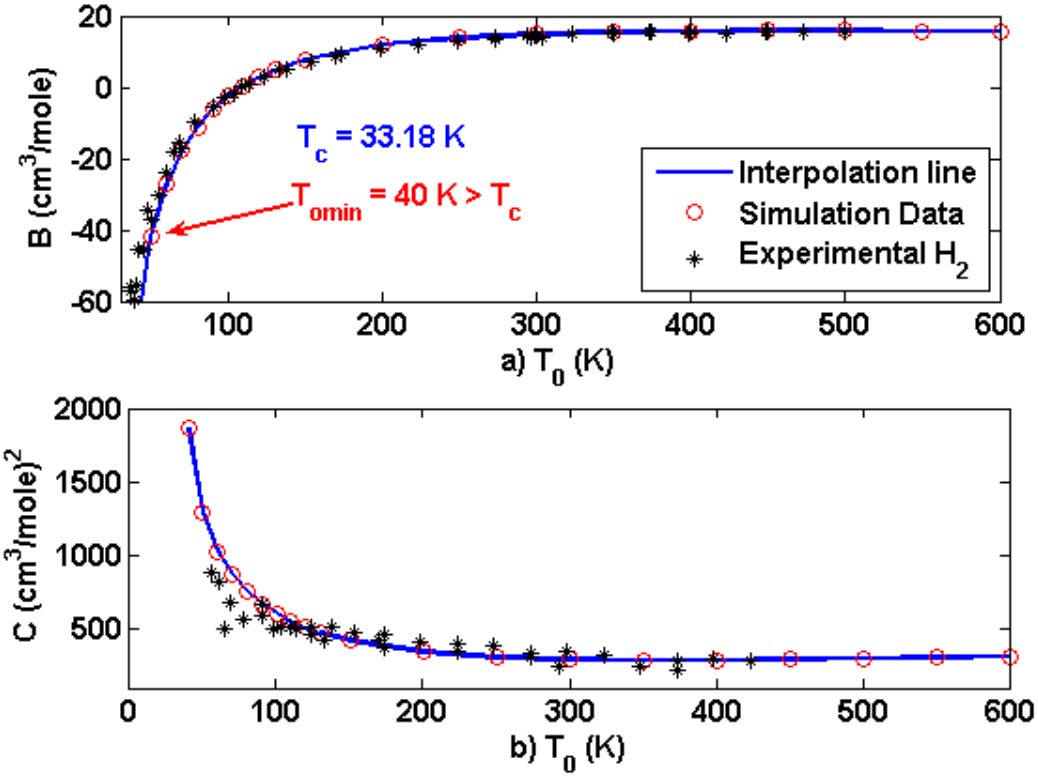

Fig. 19 a) Estimation of second virial coefficient for the hydrogen at temperatures above the critical one. b) Estimation of the third virial coefficient for the hydrogen.

5.4 Deuterium

The simulation data for the deuterium are twenty-one values for the temperatures T_0 between *98* K and *450* K as well as $P_1 = 35$ MPa and $P_s = 25$ MPa (both of them above the critical pressure). Taking into account Eqs (11) we choose $\delta = 0.26$, $\omega_n = 0.69$ rad/s, $b_0 = 3$ $mA^{-1}\cdot s^{-3}$ and $b_1 = 0.03$ $mA^{-1}\cdot s^{-2}$. With the previous values, K_{NL} is calculated for each temperature T_0 to obtain self-oscillating behavior when the conditions given by Eqs (15)-(17) are fulfilled. Therefore we obtain twenty-one values for K_{NL} between $6.412\cdot10^5$ and $4.7005\cdot10^6$ s^{-6} with $\tau_i = 300$ s.

The time constant T_m of the pressure probe is varied harmonically as shown in Eq (27) taking $\omega_{Tm} = 0.8$ rad/s, twenty-one values for T_{mv} between *5* s and *10* s and other twenty-four values for A_{Tm} between *4.1667* s and *5.5556* s. The simulation is

carried out by using the SRK equation of state (see Appendix) with a simulation step of T = 0.02 s taking $f_M = 15$, $f_P = 1.1$, $fFv = 0.68$ and $feFv = 5$ in Eqs (45) (see table 3). The estimated values for B and C are shown in Fig 20 a) and b), whereas Fig 20 c) shows the exponent *n* of the Mie intermolecular potential calculated from Eq (46). The mean value of *n* is 12.1814, which is compatible with the Lennard-Jones intermolecular potential of Eq (36). On the other hand, Fig 20 d) shows the chaotic displacement of the dimensionless valve plug as a function of the time, which allows to appreciate small time intervals where the valve remains closed.

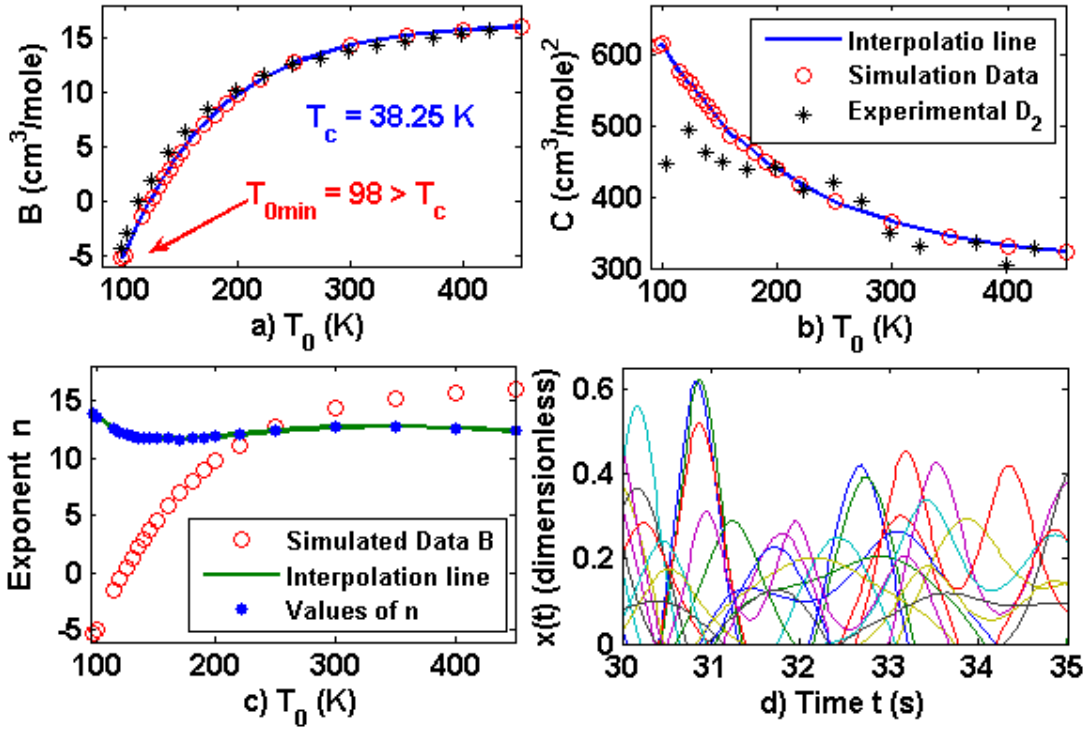

Fig. 20 a) Estimation of the second virial coefficient for the deuterium at temperatures above the critical one. b) Estimation of the third virial coefficient for the deuterium. c) Simulation data of the virial coefficient B for the deuterium and estimated values for the exponent *n* of the intermolecular potential given by Eq (44). d) Chaotic oscillations of the dimensionless valve plug displacement as a function of the time.

5.5 Neon

The simulation data for the neon consist of twenty-seven values for the temperatures T_0 between *50* K and *900* K as well as $P_1 = 20$ MPa and $P_s = 15$ MPa (both of them above the critical pressure). Taking into account Eqs (11) we choose $\delta = 0.26$, $\omega_n = 0.69$ rad/s, $b_0 = 3$ $mA^{-1}\cdot s^{-3}$ and $b_1 = 0.03$ $mA^{-1}\cdot s^{-2}$. With the previous values,

K_{NL} is calculated for each temperature T_0 to obtain self-oscillating behavior when the conditions given by Eqs (15)-(17) are fulfilled. Therefore we obtain twenty-one values for K_{NL} between $2.69 \cdot 10^4$ and $1.6216 \cdot 10^6$ s^{-6} with $\tau_i = 300$ s. The time constant T_m of the pressure probe is varied harmonically as shown in Eq (27) taking $\omega_{Tm} = 0.8$ rad/s, twenty-one values for T_{mv} between *5* s and *10* s and other twenty-four values for A_{Tm} between *4.1667* s and *5.5556* s. The simulation is carried out by using the PR equation of state (see Appendix) with a simulation step of T = 0.02 s and taking $f_M = 0.08$, $f_P = 0.9$, $fFv = 0.3$ and $feFv = 4$ in Eqs (45) (see Table 3).

The estimated values for B and C are shown in Figs 21 a) and b), whereas Fig 21 c) shows the exponent *n* of the Mie intermolecular potential with values ranging from 22.8556 to 10.6529 with a mean value of 11.0279. Such values for *n* have been calculated taking into account the values of B (which are also plotted) obtained in accordance with Eq (50).

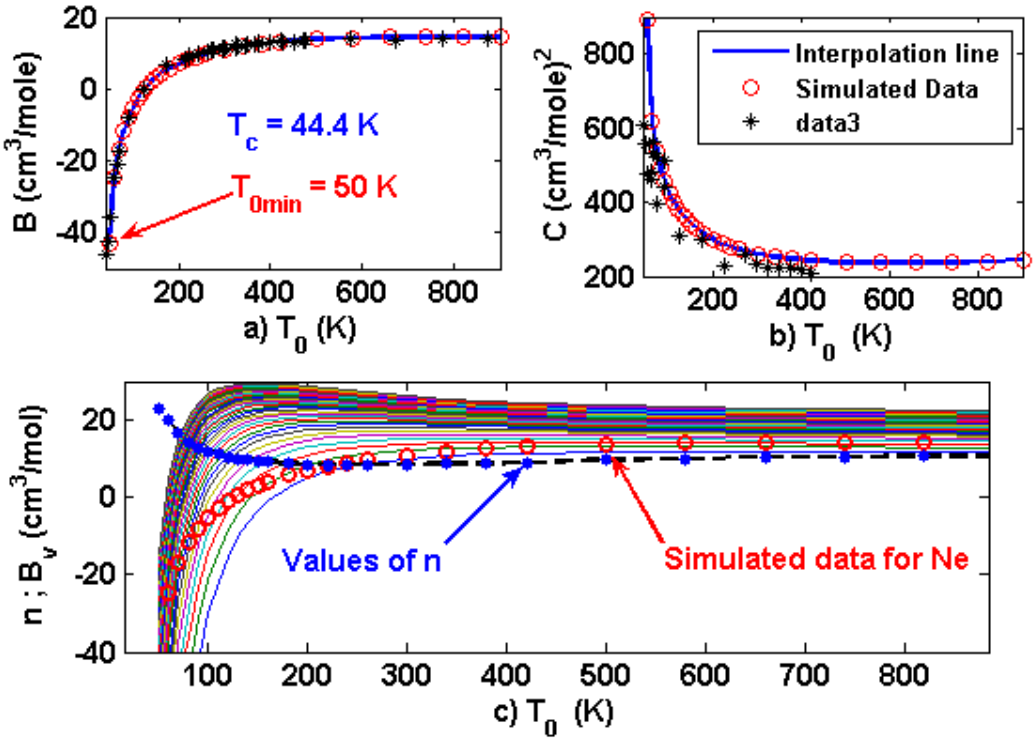

Fig. 21 a) Estimation of the second virial coefficient for the neon at temperatures above the critical one. b) Estimation of the third virial coefficient for the neon. c) Second virial coefficient for different values of the Mie intermolecular potential exponent.

It should be remarked that the Lennard-Jones parameters σ and ε used in the Mie potential play an important role in the estimation of the virial coefficients for quantum gases. For this reason, we shall analyze the quality of σ and ε by applying the generalized Mie potential given by Eqs (44) and (45) together with the theoretical estimation of virial coefficient B defined in Eq (48). This procedure aims to determine the values of σ and ε as functions of the temperature, taking into account the exponent n(T) of the Mie potential given in Eq (44) as shown in Fig 21 c) for Ne.

Assuming that the values of B obtained from the chaotic simulation data approximate the theoretical values of B given by equation (48), the following relation holds:

$$\left(\frac{B\left[T_2,n\left(T_2\right)\right]}{B\left[T_1,n\left(T_1\right)\right]}\right)_{simulated}\approx\left(\frac{B\left[T_2,n\left(T_2\right)\right]}{B\left[T_1,n\left(T_1\right)\right]}\right)_{theoretical} \tag{56}$$

where the subscripts *simulated* and *theoretical* respectively indicate the use of chaotic simulated data and Eq (50). Now assigning to ε the experimental value of the Lennard-Jones potential, Eq (50) allows to calculate σ for different values of T_1 and T_2, where T_1 is the minimum value of the input temperature T_0 and T_2 ranges between T_1 and the maximum value of T_0. The same procedure can be applied interchanging σ by ε, which allows estimating ε at different temperatures. It should be noted that, since the term $du\left(r,T\right)/dr$ under the integral of Eq (50) is proportional to ε, the relation $B\left[T_2,n\left(T_2\right)\right]/B\left[T_1,n\left(T_1\right)\right]$ only involves the parameter ε in the exponent $\exp\left[-u\left(r,T\right)/k_BT\right]$, which attenuates the dependence on ε to some extent.

Fig 22 a) shows the estimated values for σ as functions of the input temperatures T_0 together with the experimental values indicated in the legend, taking into account the estimated values of the virial coefficient B for He4, H_2, Ne and D_2. The case for He3 has not been plotted since the temperature range is very small (between 5.5 K and 30 K as shown in Fig 18 a)). The averages of the simulated values of σ for He4, H_2 Ne and D_2 are $2.5026\cdot10^{-10}$, $4.0247\cdot10^{-10}$, $2.7714\cdot10^{-10}$ and $2.8594\cdot10^{-10}$ m respectively, whose relative errors respect to the experimental values are 1.8969 %, 42.3653 %, 1.7223 %, and 2.3438 %. Consequently, the values of σ can be regarded as adequate except for H_2.

Such discrepancy for H_2 also appears for He3, and it is due to the fact that the mean value of *n* for both gases in table 3 is far away from 12 (value for the Lennard-Jones potential). On the other hand, Fig 22 b) shows the results for the parameter ε. In this case, the averages of the simulated values of ε for He4, H_2 Ne and D_2 are $1.4128 \cdot 10^{-22}$, $8.3803 \cdot 10^{-22}$, $4.5065 \cdot 10^{-22}$ and $5.1170 \cdot 10^{-22}$ J respectively, which are very close to the experimental values. Indeed, the relative errors between the previous values and the experimental results are 0.1233 %, 1.6710 %, 0.1228 %, and 0.1681 %.

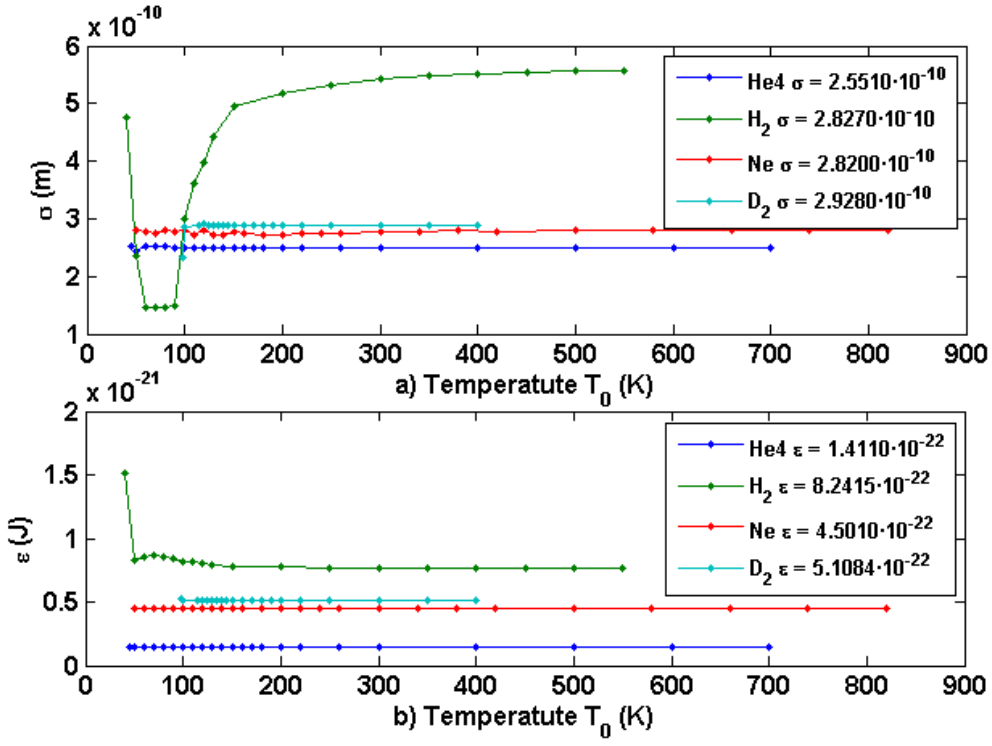

Fig. 22 a) Parameter σ used in the Mie Potential as a function of the gas input temperature T_0. b) Parameter ε used in the Mie Potential as a function of the gas input temperature T_0.

An important aspect related to the methodology summarized in the flowchart of Fig 13 is that the presence of chaotic oscillations is essential to achieve a good estimation of the virial coefficients *B(T)* and *C(T)*. To corroborate this assertion we shall consider the estimation of the virial coefficients for the Helium 4, which is a particularly interesting case (see Figs 14 and 15). For this purpose we consider twenty values for the temperatures T_0 between *45* and *800* K, as well as $P_1 = 10$ MPa, $P_s = 7$ MPa (both of them above the critical pressure) and $V = 10^{-3}$ m^3. Furthermore, taking into account Eqs (11) we choose $\delta = 0.26$, $\omega_n = 0.69$ rad/s, $b_0 = 3$ $mA^{-1} \cdot s^{-3}$, $b_1 = 0.03$ $mA^{-1} \cdot s^{-2}$ and a constant value $K_{NL} = 8.4146$ $(1/mA^2 \cdot s^6)$. With such parameters, the conditions for the appearance of a weak focus given by Eqs (15)-(17) are no longer

fulfilled. In addition, the harmonic variation of the time constant of the pressure probe given by Eq (27) is eliminated by taking a constant value T_m = 30 s for each input temperature T_0.

Figs 23 a) and b) depict the simulation results for the pressure $P_2(t)$ and the temperature $T(t)$ showing that the chaotic regime has completely disappeared and that a new self-oscillating behavior appears. In this situation, Figs 23 c) and d) show that the estimations of $B(T)$ and $C(T)$ are much worse than the previously obtained in Fig 15.

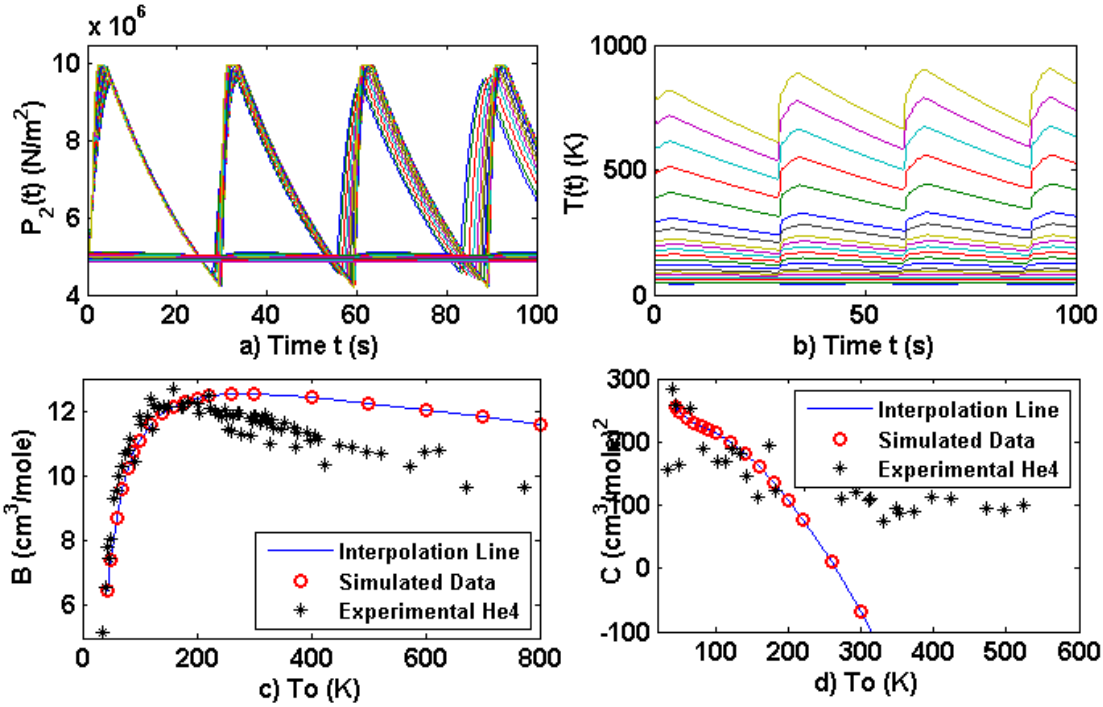

Fig. 23 a) Self-oscillating behavior of the pressure at the output of the control valve for Helium 4. b) Self-oscillating temperatures of the gas inside the vessel ranging from 45 to 800 K. c) Experimental and estimated values for the second virial coefficient B for Helium 4 obtained from non-chaotic oscillations. d) Experimental and estimated values for the third virial coefficient C for Helium 4 obtained from non-chaotic oscillations.

6 Conclusions

In this paper, a theoretical device has been analyzed at low and high pressures to obtain self-oscillating and chaotic behaviors which have been used to estimate the second and third virial coefficients of several real gases including quantum gases. The device is formed by a mechanical subsystem including a PI controller and a control

valve connected to a thermal subsystem, which is formed by an accumulation vessel and connection pipes.

The thermodynamic model of the control valve, PI controller, pressure probe and thermal subsystem has been defined by six nonlinear differential equations with one-way coupling from the mechanical subsystem to the thermal one. From a set of physically meaningful parameter values it has been verified that the mechanical subsystem can reach a self-oscillating behavior assuming cubic and high precision equations of state.

By treating the P-V-T simulation results (pressures, volumes and temperatures) obtained with the SRK equation of state as if were experimental, the second and third virial coefficients have been estimated and compared with the experimental data for the methane and argon. It has been shown that the self-oscillating behavior provides a proper estimation of the second virial coefficient in some ranges of temperature but a significant error in the third viral coefficient. Such estimation error is due to the oscillating (non constant) temperatures in the accumulator vessel as well as the periodicity in the pressures and gas densities measured by the pressure probe. To overcome such issues, the variability of the simulated data has been increased by leading the system to a chaotic regime and maintaining the accumulator vessel temperatures nearly constant by increasing its volume.

The chaotic behavior has been obtained from the self-oscillation conditions by introducing a harmonic disturbance in the time constant of the pressure probe. With this procedure, the estimation of the second and third virial coefficients is better in a wide range of temperatures, which demonstrates that the chaotic behavior provides a better fit to experimental data than the one provided by the self-oscillating behavior.

The device in chaotic regime has also been used to estimate the second virial coefficient of a mixture of gases (dry air) by using a high precision equation of state and assuming an intermolecular potential of Lennard-Jones to calculate the interaction coefficients of the mixture. It has been shown that the simulation data are very close to the experimental results for the second virial coefficient at temperatures above and below the critical one.

The methodology used in the paper has been extended to quantum gases (H4, He3, H_2, D_2, Ne) by using the effective critical constants modified by a parameterized temperature dependent function with the same form for all quantum gases. The purpose of such function relies on using cubic equations of state to estimate the second and third virial coefficients. In this sense, simple cubic equations have been investigated showing that, in all cases, the estimation of the second virial coefficient is in good agreement with the experimental data and the third virial coefficient is acceptable in some ranges of temperature. In addition, the radial distribution function has been also investigated taking into account an intermolecular potential of Mie type.

This manuscript has provided a very simple device which not requires a control system to maintain a nearly constant temperature in accumulator vessel and that can be applied to investigate different equations of state for real gases as well as their mixtures. In adition, the theoretical system presented in this work could be used to calculate the thermodynamic properties of real gases and their mixtures from the knowledge of the second and third virial coefficients calculated from the P-V-T data obtained with any equation of state.

Regarding the choice of an equation of state for a given gas (specially in the absence of experimental data), the multiparametric equations of state based on Helmholtz energy are the best available equations and generally provide the best simulation results. However, these equations are complex to implement in the simulation process and the parameter values they involve are not always known for all gases. For this reason, cubic equations of state can be an advantageous alternative, and indeed they provide good results in the estimation of *B(T)* and *C(T)* for quantum gases, as it has been verified in this work.

Finally, the main advantages of the methodology considered in this work can be summarized as follows. i) It can be used for the estimation of the second and third virial coefficients, both for individual gases and mixtures by using a computational program which can be applied with any equation of state. ii) The method is flexible, rapid and economic. iii) It is possible to estimate the virial coefficients B and C in temperature ranges for which there are no experimental data. iv) The methodology used in this paper

shows that it is possible to compare the relative error for the pressure by using several equations of state in different pressure ranges. v) The methodology can be applied with good results for quantum gases by using very simple modified cubic equations.

References

[dataset] [1] Emerson Process Management, Control Valve Handbook. fourth ed. http://www.documentation.emersonprocess.com/groups/public/documents/book/cvh99.pdf, 2012.

[dataset] [2] Metso Automatic Inc, Flow control manual. Vanha Porvoontie, sixthed.Finland.http://valveproducts.metso.com/documents/softwarepackages/nelprof/FlowControl_manual.pdf, 2011.

[3] J. W. Hutchinson, ISA Handbook of Control Valves, second ed. Instrument Society of America. Research Triangle Park, D.C., U.S.A, 1976.

[4] K. Ogata, Systems Dynamics, first ed., Prentice Hall, New York, 1980.

[dataset]

[5] Desin instrument series BS-2100, BS-2200, BS-2300, BS-2400, BS-2500, http://www.electroson.com/documentos/D_BS2500LLC_0_DESIN_BS2500_PDF.pdf, 2015.

[6] D. P. Tassios, Applied Chemical Engineering Thermodynamics, Springer-Verlag, Berlin Heidelberg, 1993.

[7] I. G. Economou, Cubic and Generalized van der Waals Equations of state in: A. R. H. Goodwin, J. V. Sengers, C. J. Peters (Eds.), Applied Thermodynamics of Fluids, 2010, pp. 53-83.

[8] Eric W. Lemmon, Roland Span, Multi-parameter Equations of State for Pure Fluids and Mixtures in: A. R. H. Goodwin, J. V. Sengers, C. J. Peters (Eds.), Applied Thermodynamics of Fluids, 2010, pp. 394-432.

[9] J. Gmehling, B. Kolbe, M. Kleiber, J. Rarey, Chemical Thermodynamics, Wiley-VCH, 2012.

[10] M. Pérez-Molina, J. Gil-Chica, E. Fernández-Varó, M. F. Pérez-Polo, Commun. Nonlinear Sci. Numer. Simulat. 36 (2016) 468–495.

[11] M. F. Pérez-Polo, M. Pérez-Molina, E. Fernández-Varó, J. Gil-Chica, Chem. Eng. Sci. 155, (2016) 482-503.

[12] J. Guckenheimer, P. Holmes, Nonlinear Oscillations, Dynamical Systems and Bifurcations of Vector Fields, Springer, New York, 1983.

[13] S. Wiggins, Introduction to Applied Nonlinear Dynamical Systems and Chaos, second ed.. Springer, New York, 2000.

[14] L. P. Shilnikov, A. L. Shilnikov, D.V. Turaev, L. O. Chua. Methods of Qualitative Theory in Nonlinear Dynamics. Part II, World Scientific, New Jersey, 2001.

[15] B. E. Poling, J. M. Prausnitz, J. P. O'Connell, The Properties of Gases and Liquids, fifth ed., Mc-Graw Hill, New York, 2001.

[16] J. M. Prausnitz, R. N. Lichtenthaler, E. Gomes de Azevedo, Molecular Thermodynamics of Fluid-Phse Equilibria, third ed., Prentice Hall, New York, 2000

[17] D.-Y. Peng, D.B. Robinson, Ind. Eng. Chem. Fundam. 15 (1) (1976) 59–64.

[18] J. S. Lopez-Echeverry, S. Reif-Acherman, E. Araujo-Lopez, Fluid Phase Equilib. 447 (2017) 39-71.

[19] G. Soave, Chem. Eng. Sci. 27 (6) (1972) 1197–1203.
[20] R. Privat, Y. Privat, J.-N. Jaubert, Fluid Phase Equilib. 282 (2009) 38–50
[21] G. Soave,Chem. Eng. Sci. 39 (1984) 345-350.
[22] M. M. Abbot, Cubic Equation of State: An Interpretive Review. Equations of State in Engineering and Research. Adv. In Chem. Ser. 182 K. C. Chao, R. L. Robinson eds. American Chemical Society, Washington, 1979.
[23] A. I. Gosman, R. D. McCarty, J. G. Hust, Thermodynamic Properties of Argon. From the Triple Point to 300 K at Pressures up to 1000 Atmospheres, Cryogenic Division. Institute for Basic Standars NSRDS 1-32, 1969.
[24] C. L. Yaws, Chemical Properties Handbook, McGraw-Hill, New York, 1999.
[25] O. A. Hougen, K. M. Watson, R. A. Ragatz, Industrial Chemical Calculations, Vol. II Thermodynamics, second ed., John Wiley & Sons, New York, 1954.
[26] T. L. Hill, Statistical Mechanics: Principles and Selected Applications. Dover, New York, 2003.
[27] J. H. Dymond, K. N. Marsh, R. C. Wilhoit, K. C. Wong, Virial Coefficients of Pure Gases and Mixtures, Springer_Verlag, Berlin, 2002.
[28] R.D. Gunn, P.L. Chueh, J.M. Prausnitz, AIChE J. 12 (1966) 937–941.
[29] Long Meng, Yuan-Yuan Duan, Fluid Phase Equilib. 258 (2007) 29–33.
[30] Robert D. McCarty, Thermodynamic properties of Helium 4 from 2 to 1500 K at Pressures of 10^8 Pa, J. Phys. Chem. Ref. Data 2 (1973) 923-1041.
[31] J. W. Leachman, R. T Jacobsen, S. G. Penoncello, E. W. Lemmon, J. Phys. Chem. Ref. Data. 38, (2009) 721-745.
[32] Gerald I. Kerley, Equation of state for Hydrogen and Deuterium, Sandia National Laboratories, Albuquerque, N. M., Sandia Report, Sand2003-3613, 2003.
[33] R.M.Gibbons, Cryogenics 9 (1969) 251-260.
[34] Y. Huang, G. Chem, V. Arp, J. Chem. Phys. 125 (2006) 054505.
[35] A. E. Nasrabad, R. Laghaei, and U. K. Deiters, J. of Chem. Phys. 121 (2004) 6423-6434.
[36] Eugene Holleran, Fluid Phase Equilibria 251 (2007) 29–32.

Appendix

In accordance with Eq (18), the parameters of the cubic equations are the following ones: $T_r = T/T_c$ and $P_r = P/P_c$ denote reduced temperature and pressure respectively, whereas T_c, P_c and ω are respectively the critical temperature, the critical pressure and the acentric factor of the considered gas [16-22], [24].

i) Redlich-Kwong (RK) equation of state

$$\Theta(T) = a\alpha(T_r)\ ;\ \delta_1 = b : \varepsilon = 0\ ;\ a = 0.42748\frac{(RT_c)^2}{P_c}\ ;\ b = 0.08664\frac{RT_c}{P_c}$$
$$\eta = b\ \ ;\ \ \alpha(T_r) = \frac{1}{T_r^{0.5}} \qquad \text{(A1)}$$

ii) Soave-Redlich-Kwong (SRK) equation of state

$$\Theta(T)=a\alpha(T_r)\ ;\ \delta_1=b:\varepsilon=0\ ;\ a=0.42748\frac{(RT_c)^2}{P_c}\ ;\ b=0.08664\frac{RT_c}{P_c}$$
$$\alpha(T_r)=\left[1+\left(0.48+1.574\omega-0.176\omega^2\right)\left(1-T_r^{0.5}\right)\right]^2 \quad \text{(A2)}$$

iii) Peng-Robinson (PR) equation of state

$$\Theta(T)=a\alpha(T_r)\ ;\ \delta_1=2b\ ;\ \varepsilon=-b^2\ ;\ \eta=b\ \ ;a=0.45724\frac{(RT_c)^2}{P_c}\ ;\ b=0.0778\frac{RT_c}{P_c}$$
$$\alpha(T_r)=\left[1+\left(0.37464+1.5423\omega-0.2669\omega^2\right)\left(1-T_r^{0.5}\right)\right]^2$$
(A3)

iv) Soave (S) equation of state

$$\Theta(T)=a\alpha(T_r)\ ;\ \delta_1=b\ ;\ \varepsilon=0.001736\left(\frac{RT_c}{P_c}\right)^2$$
$$a=0.42118\frac{(RT_c)^2}{P_c}\ ;\ b=0.08333\frac{RT_c}{P_c} \quad \text{(A4)}$$
$$\alpha(T_r)=\left[1+\left(0.4998+1.5928\omega-0.19563\omega^2+0.025\omega^3\right)\left(1-T_r^{0.5}\right)\right]^2$$

v) Peng-Robinson equation of state with translation volume (PRT)

$$\Theta(T)=a\alpha(T_r)\ ;\ \delta_1=2(t+b):\varepsilon=t^2\ ;\ \eta=b\ ;\ a=0.45724\frac{(RT_c)^2}{P_c}\ ;\ b=0.0778\frac{RT_c}{P_c}$$
$$m_t=0.384401+1.522760\omega-0.213808\omega^2+0.034616\omega^3-0.001976\omega^4$$
$$\alpha(T_r)=\left[1+m_t\left(1-T_r^{0.5}\right)\right]^2$$
$$t_0=\frac{RT_c}{P_c}\left(-0.014471+0.067498\omega-0.084852\omega^2+0.067298\omega^3-0.017366\omega^4\right)$$
$$t_1=\frac{RT_c}{P_c}\left[\left(\frac{3}{8}\right)-z_c\right]\ ;\ \beta=-10.244700-28.631200\omega\ ;\ t=t_0+(t_1-t_0)\exp\left[\beta\left|1-T_c\right|\right]$$
(A5)

where z_c is the critical compressibility coefficient. In this case, the equation of state can be written as:

$$P=\frac{RT}{v+t-b}-\frac{a\alpha(T_r)}{(v+t)(v+t+b)+b(v+t-b)} \quad \text{(A6)}$$

vi) Van-der-Waals equation of state with translation volume (VDWT)

$$\Theta(T)=a\alpha(T_r)\ ;\ \delta_1=2(t+b)\ \ ;\ \ \varepsilon=t^2\ \ ;\ a=\frac{27}{64}\frac{(RT_c)^2}{P_c}\ ;\ b=\frac{1}{8}\frac{RT_c}{P_c}$$

$$m_t=0.48523+1.62400\omega-0.21884\omega^2\ \ ;\ \ \alpha(T_r)=\left[1+m_t\left(1-T_r^{0.5}\right)\right]^2$$

$$t_0=\frac{RT_c}{P_c}\left(0.0348+0.0937\omega-0.1661\omega^2+0.1250\omega^3\right) \qquad \text{(A7)}$$

$$t_1=\frac{RT_c}{P_c}\left[\frac{3}{8}-z_c\right]\ \ ;\ \ z_c=0.2890-0.0701\omega-0.0207\omega^2$$

$$\beta=10.244700-28.631200\omega\ \ ;\ \ t=t_0+(t_1-t_0)\exp\left[\beta\left|1-T_c\right|\right]$$

The equation of state can be written as:

$$P=\frac{RT}{v+t-b}-\frac{a\alpha(T_r)}{(v+t)^2} \qquad \text{(A8)}$$

Highlights

- Theoretical device for virial coefficient estimation through chaotic behavior
- High precision equation of state to obtain virial coefficient B of dry air
- Virial coefficients of quantum gases by using modified cubic equations of state
- Analysis of the intermolecular potential from chaotic simulation data
- Estimation of the radial distribution function for quantum gases